**Figure 3**

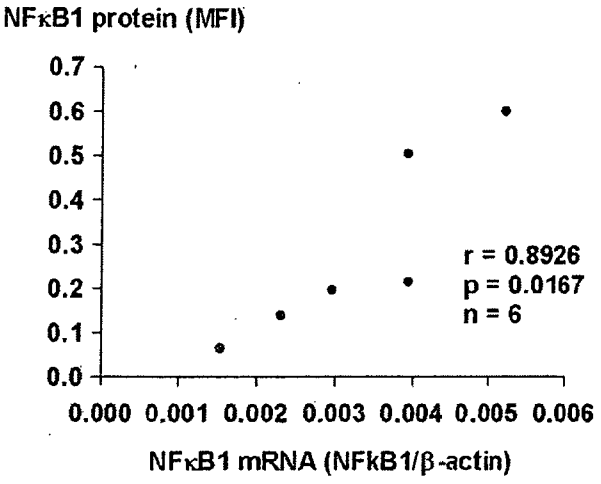


Comparison of the expression of nuclear factor (NF)κB1 (p50) protein with that of NFκB1 mRNA in bone marrow CD34+ cells. Purified bone marrow CD34+ cells were permeabilized and then stained with phychoerythrin-conjugated anti-NFκB p50 monoclonal antibody or phychoerythrin-conjugated normal mouse IgG1, followed by analysis with flow cytometry. The NFκB1 protein levels as expressed by mean fluorescence intensity were compared with NFκB1 mRNA levels (expressed as the ratio of the mRNA copy numbers to those of β-actin) in bone marrow CD34+ cells from six patients (three rheumatoid arthritis patients and three osteoarthritis patients). Statistical significance was evaluated by linear regression test.

**Figure 4**

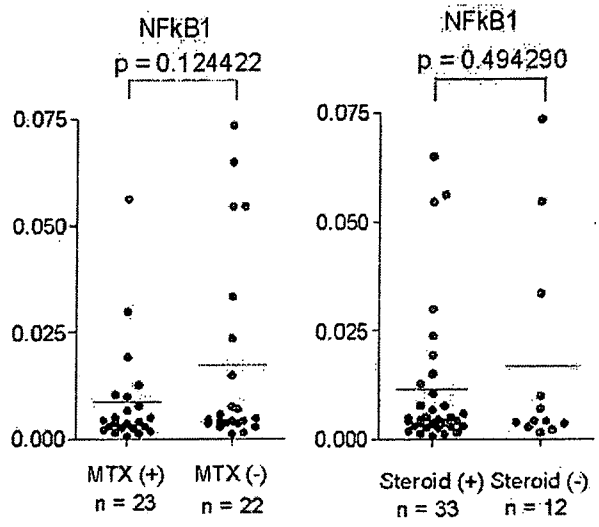


The relevance of treatment with the expression of mRNAs for nuclear factor (NF)κB1 mRNA in bone marrow CD34+ cells. Total RNA was isolated from purified bone marrow CD34+ cells from 45 rheumatoid arthritis patients. The expression of mRNAs for NFκB1 and β-actin was evaluated by real-time quantitative PCR. The data are expressed as the ratio of the mRNA copy numbers to those of β-actin. Effect of treatment with methotrexate (MTX) or oral steroids (Steroid) was evaluated by Welch's *t* test. Horizontal lines indicate the mean values.

48 hours and then harvested for RNA extraction. Alternatively, the cells were cultured in a 24-well microtiter plate at $2 \times 10^5$ cells per well in 1.0 ml culture medium for 4 weeks in the presence of SCF (10 ng/ml), GM-CSF (1 ng/ml) and TNF-α (10 ng/ml) without medium change, as previously described [2]. The differentiation of fibroblast-like cells was observed under the phase-contrast light microscopy. The concentrations of MMP-1 and vascular endothelial growth factor (VEGF) in the culture supernatants were measured using the Biotrak human MMP-1 ELISA system (Amarsham Pharmacia Biotech, Buckinghamshire, UK) and human VEGF immunoassay kit (BioSource International, Camarillo, CA, USA), respectively. The concentrations of $\beta_2$-microglobulin ($\beta_2$MG) were determined by an ELISA as previously described [6].

### Statistics

Comparison between RA and OA patients and between RA patients with MTX or steroid and those without MTX or steroid was carried out using Welch's *t* test. Significance of the effects of siRNA transfection on the generation of fibroblast-like cells and on the production of MMP-1 and VEGF was evaluated by Wilcoxon's signed rank test. Correlation between serum C-reactive protein and NFκB1 mRNA in bone marrow CD34+ cells and that between NFκB1 mRNA and protein were evaluated using a liner regression test. Correlation between NFκB1 mRNA in bone marrow CD34+ cells and the generation of fibroblast-like cells was analyzed using a Spearman's rank correlation test.

## Results

### Expression of mRNAs for various components of NFκB in bone narrow CD34+ cells

The expression of mRNA for NFκB1 (p50), NFκB2 (p52), and RelA (p65) in bone marrow CD34+ cells is shown as the ratio of the copy numbers to those of β-actin mRNA in Figure 1. The expression of NFκB1 mRNA was significantly higher in RA bone marrow CD34+ cells than in OA bone marrow CD34+ cells ($p = 0.005351$), whereas there were no significant differences in the expression of NFκB2 mRNA ($p = 0.130116$). Although the expression of RelA mRNA appeared to be lower in RA bone marrow CD34+ cells than in OA bone marrow CD34+ cells, it did not reach statistical significance ($p = 0.192150$). These results indicate that the expression of mRNA for components of NFκB1 is exclusively enhanced in bone marrow CD34+ cells from patients with RA.

Next, experiments were carried out to examine whether the elevation of NFκB1 mRNA expression parallels the elevation of NFκB1 protein expression in bone marrow CD34+ cells. The protein expression of NFκB1 was evaluated by staining of permeabilized bone marrow CD34+ cells from three RA patients and three OA patients with anti-NFκB p50 monoclonal antibody, followed by analysis with flow cytometry. As can be seen

**Figure 5**

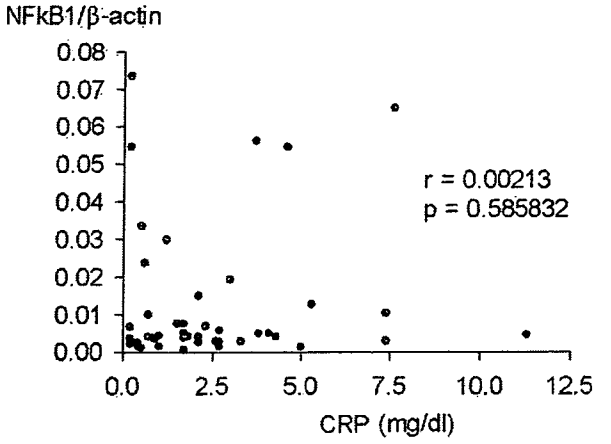


The correlation of the expression of mRNAs for nuclear factor (NF)κB1 mRNA in bone marrow CD34+ cells with serum C-reactive protein (CRP). Total RNA was isolated from purified bone marrow CD34+ cells from 45 rheumatoid arthritis patients. The expression of mRNAs for NFκB1 and β-actin was evaluated by real-time quantitative PCR. The data are expressed as the ratio of the mRNA copy numbers to those of β-actin. Statistical significance was evaluated by linear regression test.

in Figure 2, bone marrow CD34+ cells express NFκB1 (p50) protein, the quantity of which can be expressed as MFI. Moreover, there is significant correlation between MFI for NFκB1 and NFκB1 mRNA in the six bone marrow CD34+ cells (Figure 3). The results indicate that the elevation of NFκB1 mRNA leads to the increase in NFκB1 protein expression.

### Relevance of expression of NFκB1 mRNA in bone marrow CD34+ cells from RA patients to treatment and clinical parameters

Of note, 22 and 33 of the 45 RA patients were treated with MTX and oral steroids, respectively, whereas no OA patients were taking either MTX or oral steroids. It is therefore possible that MTX and oral steroids might have affected the expression of NFκB1 mRNA in bone marrow CD34+ cells. As shown in Figure 4, however, there were no significant differences in the expression of NFκB1 mRNA in bone marrow CD34+ cells between RA patients taking MTX or oral steroids and those who were not, although the expression of NFκB1 mRNA appeared to be lower in RA patients taking MTX or oral steroids. It is unlikely, therefore, that the medication the RA patients were taking would have resulted in the upregulation of NFκB1 mRNA expression in bone marrow CD34+ cells. It should be also noted that the expression of NFκB1 mRNA in bone marrow CD34+ cells was not significantly correlated with serum C-reactive protein (CRP) levels in RA patients (Figure 5). The data thus indicate that the upregulation of NFκB1 mRNA in bone marrow CD34+ cells is independent of the activity of the systemic inflammation, as reflected by serum CRP.

**Figure 6**

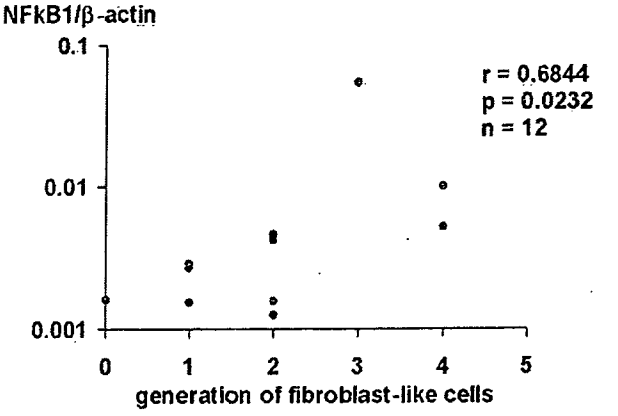


Comparison of the expression of nuclear factor (NF)κB1 (p50) mRNA in bone marrow CD34+ cells with their capacity to differentiate into fibroblast-like cells. The expression of NFκB1 mRNA in bone marrow CD34+ cells from 12 rheumatoid arthritis patients was evaluated by real-time quantitative PCR prior to the culture. The bone marrow CD34+ cells were incubated in culture medium with stem cell factor (10 ng/ml), granulocyte-macrophage colony stimulating factor (1 ng/ml) and tumor necrosis factor-α (10 ng/ml) for 4 weeks with no medium changes. Morphological changes were evaluated under light microscopy. The percentages of fibroblast-like cells were calculated from two view fields at ×20 magnifications. The degree of the generation of fibroblast-like cells were scored as follows: 0, fibroblast-like cells <5%; 1, fibroblast-like cells 5% to 25%; 2, fibroblast-like cells 25% to 50%; 3, fibroblast-like cells >50%; 4, formation of a pile or a cluster in at least one view field. Statistical significance was evaluated by Spearman's rank correlation test.

### Relevance of the expression of NFκB1 mRNA to the generation of fibroblast-like cells

There was a variation in the expression of NFκB1 mRNA among the RA patients. We next examined the relationship of the initial levels of NFκB1 mRNA in RA bone marrow CD34+ cells with their capacity to differentiate into fibroblast-like cells. As shown in Figure 6, there was a significant correlation between the NFκB1 mRNA expression and the generation of fibroblast-like cells from bone marrow CD34+ cells upon stimulation with SCF, GM-CSF and TNF-α for 4 weeks in 12 RA patients. The data indicate that the enhanced expression of NFκB1 mRNA is important for the enhanced generation of fibroblast-like cells.

### Effect of TNF-α on the expression of mRNAs for various components of NFκB in bone marrow CD34+ cells

Previous studies have demonstrated that TNF-α plays a critical role in the pathogenesis of RA [4]. It is possible, therefore, that the up-regulation of NFκB1 mRNA in bone marrow CD34+ cells might be secondary to the increased levels of TNF-α in the born marrow; experiments were carried out to test this possibility. Highly purified bone marrow CD34+ cells from healthy individuals were cultured in the presence of TNF-α (10 ng/ml) for 24 hours, after which the expression of mRNA for various components of NFκB was examined. As shown in Fig-

**Figure 7**

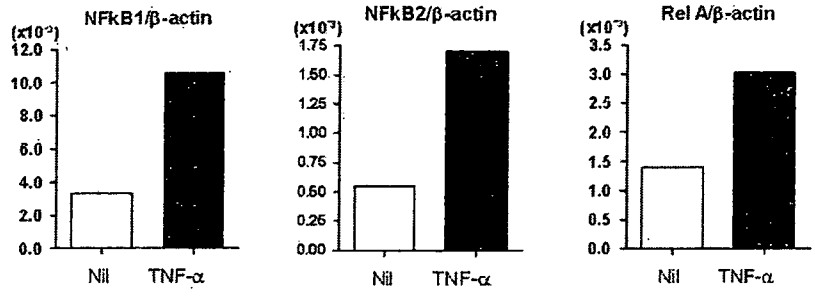


Effect of tumor necrosis factor (TNF)-α on the expression of mRNAs for nuclear factor (NF)κB1 (p50), NFκB2 (p52) and RelA (p65) in bone marrow CD34+ cells. Bone marrow CD34+ cells from healthy individuals were incubated in culture medium with or without TNF-α (10 ng/ml) for 24 hours. After the incubation, total RNA was isolated for evaluation of the expression of mRNAs for NFκB1, NFκB2, RelA and β-actin by real-time quantitative PCR. The data are expressed as the ratio of the mRNA copy numbers to those of β-actin. The data are representative of two different experiments.

ure 7, treatment of bone marrow CD34+ cells with TNF-α upregulated not only the expression of NFκB1 (p50) mRNA, but that of NFκB2 (p52) mRNA and RelA (p65) mRNA. Since only the expression of NFκB1 mRNA, but not that of NFκB2 mRNA and RelA mRNA, was significantly upregulated in RA bone marrow CD34+ cells, the increased expression of NFκB1 mRNA in RA bone marrow CD34+ cells might not be accounted for simply by the increased levels of TNF-α in the bone marrow.

**Figure 8**

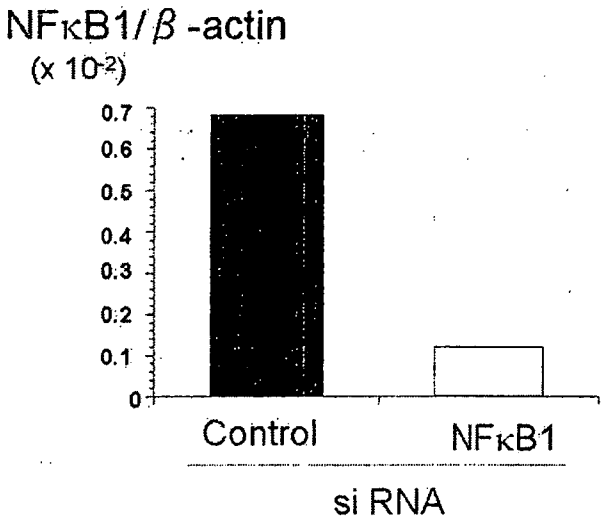


Silencing of nuclear factor (NF)κB1 mRNA in bone marrow CD34+ cells by small interfering RNA (siRNA) for NFκB1. Purified bone marrow CD34+ cells were transfected with siRNA for NFκB1 or a scrambled sequence control siRNA after a 24 hours incubation in culture medium with stem cell factor (10 ng/ml) and granulocyte-macrophage colony stimulating factor (1 ng/ml). After the transfection, the cells were further incubated for 48 hours in culture medium with stem cell factor and granulocyte-macrophage colony stimulating factor, and total RNA was isolated for evaluation of the expression of NFκB1 mRNA and β-actin mRNA by real-time quantitative PCR. The data are expressed as the ratio of the mRNA copy numbers to those of β-actin.

**Effect of silencing mRNA for NFκB1 on differentiation of RA bone marrow CD34+ cells into fibroblast-like cells upon stimulation with SCF, GM-SCF and TNF-α**

We next examined whether silencing of NFκB1 (p50) mRNA in RA bone marrow CD34+ cells might correct their abnormal responses to TNF-α. As shown in Figure 8, treatment of bone marrow CD34+ cells with siRNA for NFκB1 reduced the expression of NFκB1 mRNA by approximately 80%. More importantly, reduction of NFκB1 mRNA markedly suppressed the generation of fibroblast-like cells from RA bone marrow CD34+ cells upon stimulation with SCF, GM-CSF and TNF-α (Figures 9 and 10). Accordingly, silencing of NFκB1 by siRNA

**Figure 9**

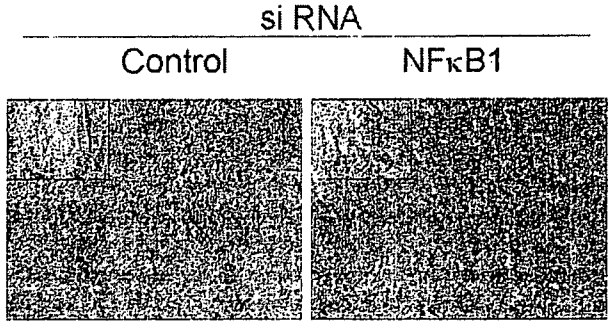


Inhibition of the generation of fibroblast-like cells by silencing nuclear factor (NF)κB1 mRNA in bone marrow CD34+ cells from patients with rheumatoid arthritis. Purified bone marrow CD34+ cells were transfected with small interfering RNA (siRNA) for NFκB1 or a scrambled sequence control, after which the cells were incubated in culture medium with stem cell factor (10 ng/ml), granulocyte-macrophage colony stimulating factor (1 ng/ml) and tumor necrosis factor-α (10 ng/ml) for 4 weeks with no medium changes. Morphological changes were observed under light microscopy (original magnification, ×20; inset, ×50 magnification). The data are representative of 12 different experiments.

**Figure 10**

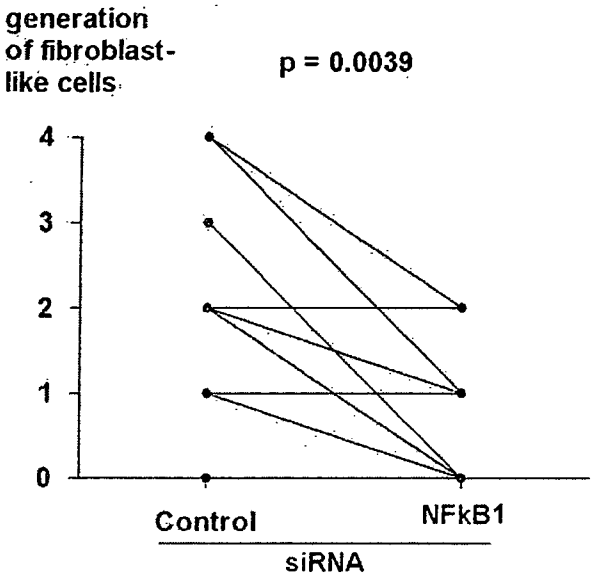


Inhibition of the generation of fibroblast-like cells by silencing nuclear factor (NF)κB1 mRNA in bone marrow CD34+ cells from patients with rheumatoid arthritis. Purified bone marrow CD34+ cells were transfected with small interfering RNA (siRNA) for NFκB1 or a scrambled sequence control siRNA, after which the cells were incubated in culture medium with stem cell factor (10 ng/ml), granulocyte-macrophage colony stimulating factor (1 ng/ml) and tumor necrosis factor-α (10 ng/ml) for 4 weeks with no medium changes. Morphological changes were observed under light microscopy. The percentages of fibroblast-like cells were calculated from two view fields at ×20 magnifications. The degree of the generation of fibroblast-like cells were scored as follows: 0, fibroblast-like cells <5%; 1, fibroblast-like cells 5% to 25%; 2, fibroblast-like cells 25% to 50%; 3, fibroblast-like cells >50%; 4, formation of a pile or a cluster in at least one view field. Statistical significance was evaluated by Wilcoxon's signed rank test.

**Figure 11**

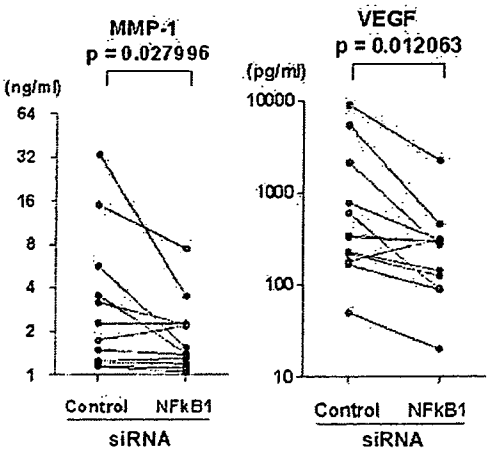


Suppression of the production of matrix metalloproteinase (MMP)-1 and vascular endothelial growth factor (VEGF) by silencing nuclear factor (NF)κB1 mRNA in bone marrow CD34+ cells from patients with rheumatoid arthritis. Purified bone marrow CD34+ cells from 12 patients with rheumatoid arthritis were transfected with small interfering RNA (siRNA) for NFκB1 or a scrambled sequence control siRNA, after which the cells were further incubated in culture medium with stem cell factor (10 ng/ml), granulocyte-macrophage colony stimulating factor (1 ng/ml) and tumor necrosis factor-α (10 ng/ml) for 4 weeks with no medium changes. After the incubation, the supernatants were harvested and assayed for MMP-1 and VEGF by ELISA. Statistical significance was evaluated by Wilcoxon's signed rank test.

significantly decreased the levels of MMP-1 and VEGF in culture supernatants of RA bone marrow CD34+ cells (Figure 11). Since bone marrow CD34+ cells proliferate in response to SCF, GM-CSF and TNF-α, it was possible that differences in MMP-1 and VEGF might be a result of alteration in cell proliferation by NFκB1 siRNA. Previous studies disclosed that $\beta_2$MG is produced by a number of cell types, including lymphocytes, myeloid cells, and tumor cells [7-9]. The production of $\beta_2$MG generally correlates with cell proliferation [6-9]. In fact, the levels of $\beta_2$MG in the culture supernatants paralleled the viable cell counts of bone marrow CD34+ cells stimulated with SCF, GM-CSF and TNF-α. Of note, silencing of NFκB1 also significantly decreased the ratios of MMP-1 and VEGF to $\beta_2$MG (MMP-1/$\beta_2$MG and VEGF/$\beta_2$MG) in culture supernatants of RA bone marrow CD34+ cells (Figure 12). Consistently, whereas siRNA for NFκB1 inhibited the differentiation of RA bone marrow CD34+ cells stimulated with SCF, GM-CSF and TNF-α into fibroblast-like cells (Figure 13), it significantly influenced neither the viable cell numbers nor the levels of $\beta_2$MG in the culture supernatants (Figure 14). These results confirm that the enhanced expression of NFκB1 mRNA in RA bone marrow CD34+ cells led to their abnormal capacity to differentiate into fibroblast-like cells producing MMP-1 upon stimulation with SCF, GM-CSF and TNF-α without affecting cell viability or proliferation. The data suggest, therefore, that the enhanced expression of NFκB1 mRNA in bone marrow hematopoietic stem cells might play a pivotal role in the pathogenesis of RA.

## Discussion

The importance of TNF-α in the pathogenesis of RA has been well appreciated. Thus, anti-TNF-α antibodies and soluble TNF receptors have been demonstrated to have beneficial effects in the treatment of RA [4]. On the other hand, increasing attention has been paid to the role of bone marrow abnormalities in the pathogenesis of RA. In this regard, we demonstrated that RA bone marrow CD34+ cells have abnormal capacities to respond to TNF-α and to differentiate into fibroblast-like cells producing MMP-1 [2]. It should be noted that NFκB plays an important role in signal transduction and expression of a variety of genes, including MMP-1, under the influence of TNF-α [3]. The results in the current study have demonstrated that the expression of mRNA for NFκB1 is increased in RA bone marrow CD34+ cells. Of note, the expression of NFκB1 mRNA was significantly correlated with that of NFκB1 protein. Moreover, the initial levels of NFκB1 mRNA in RA bone marrow CD34+ cells were correlated with

**Figure 12**

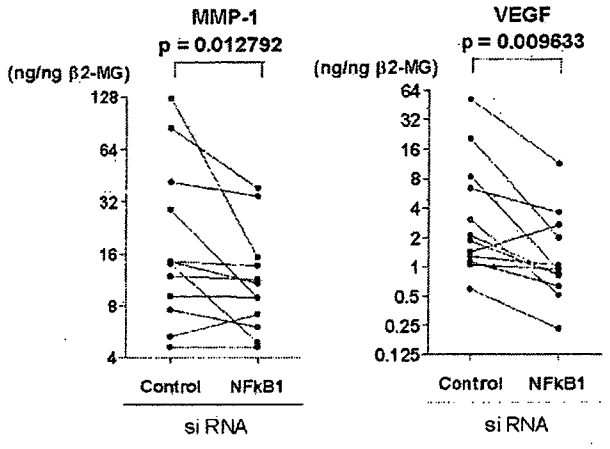


Suppression of the production of matrix metalloproteinase (MMP)-1 and vascular endothelial growth factor (VEGF) by silencing nuclear factor (NF)κB1 mRNA in bone marrow CD34+ cells from patients with rheumatoid arthritis. Purified bone marrow CD34+ cells from 12 patients with rheumatoid arthritis were transfected with small interfering RNA (siRNA) for NFκB1 or a scrambled sequence control siRNA, after which the cells were further incubated in culture medium with stem cell factor (10 ng/ml), granulocyte-macrophage colony stimulating factor (1 ng/ml) and tumor necrosis factor-α (10 ng/ml) for 4 weeks with no medium changes. After the incubation, the supernatants were harvested and assayed for MMP-1, VEGF and $\beta_2$-microglobulin ($\beta_2$MG) by ELISA. Statistical significance was evaluated by Wilcoxon's signed rank test.

their capacity to differentiate into fibroblast-like cells upon stimulation with TNF-α. The data suggest that the increased expression of NFκB1 mRNA might lead to constitutive overproduction of NFκB p50 molecules and thus result in abnormal responses to TNF-α of RA bone marrow CD34+ cells. Of note, bee venom and its major component melittin have been shown to display anti-arthritic effects through inactivation of NFκB [10]. Since bee venom and melittin delay and reduce nuclear translocation of the p50 subunit of NFκB but not p65 (RelA) [10], the importance of NFκB p50 rather than p65 in the pathogenesis of inflammatory arthritides has been underscored.

In the present study, significant numbers of RA patients were treated with MTX and oral steroids. However, there were no significant differences in the expression of NFκB1 mRNA in bone marrow CD34+ cells between RA patients receiving MTX or oral steroids and those who were not, although the expression of NFκB1 mRNA appeared to be lower in RA patients receiving these drugs. It is suggested, therefore, that administration of MTX and oral steroids might have made the differences in the expression of NFκB1 mRNA in bone marrow CD34+ cells between RA and OA less marked. On the other hand, the expression of NFκB1 mRNA in bone marrow CD34+ cells was not correlated with serum CRP levels in RA patients. The upregulation of NFκB1 mRNA in bone marrow CD34+ cells might not, therefore, be secondary to systemic inflammation, but may be a primary abnormality intrinsic to RA.

In the present study, the expression of mRNA for RelA (p65) appeared to be decreased in RA bone marrow CD34+ cells compared with that in OA bone marrow CD34+ cells, although this decrease did not reach statistical significance. Of note, a previous study demonstrated that embryonic fibroblasts from RelA-deficient mice are defective in the TNF-α mediated induction of mRNAs for IκBα [11]. Moreover, in RelA deficient fibroblasts, IκBβ protein was absent, presumably due

**Figure 13**

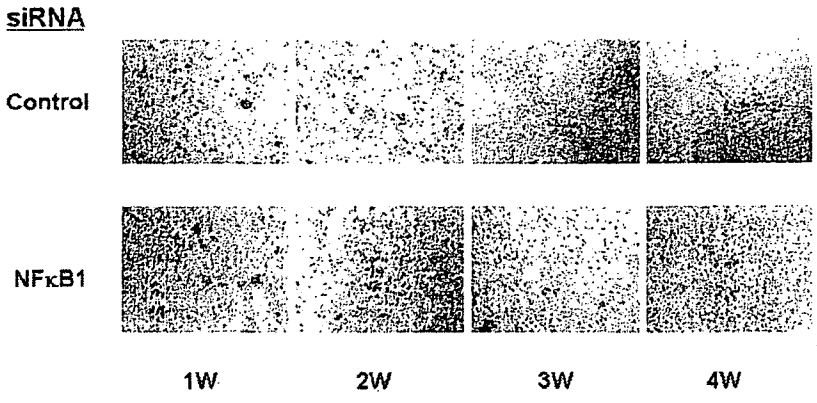


Time-kinetic effect of silencing nuclear factor (NF)κB1 mRNA in bone marrow CD34+ cells from patients with rheumatoid arthritis on the generation of fibroblast-like cells. Purified bone marrow CD34+ cells from patients with rheumatoid arthritis were transfected with small interfering RNA (siRNA) for NFκB1 or scrambled sequence control siRNA, after which the cells were further incubated in culture medium with stem cell factor (10 ng/ml), granulocyte-macrophage colony stimulating factor (1 ng/ml) and tumor necrosis factor-α (10 ng/ml) up to 4 weeks with no medium changes. After various periods of incubation (W, weeks), the morphological changes of the cells were observed under light microscopy. The data are representative of three different experiments.

**Figure 14**

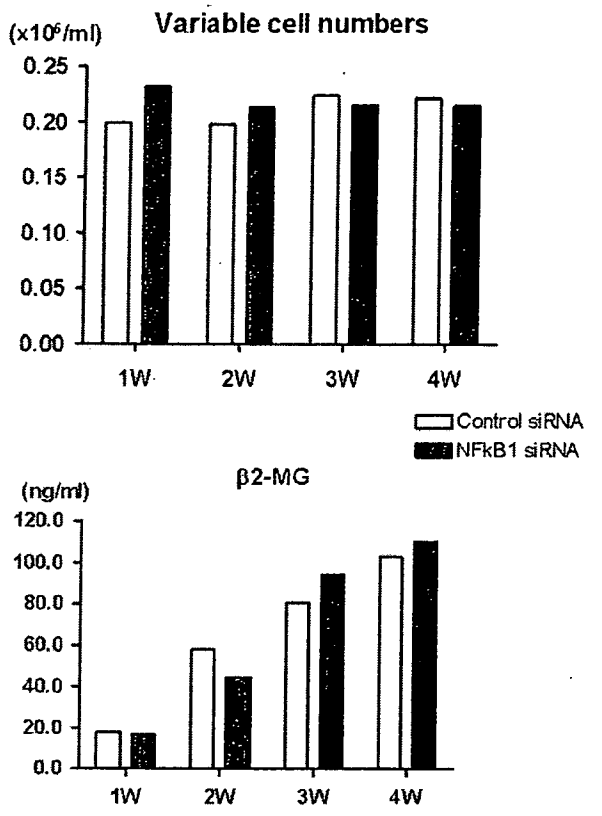


Time-kinetic effect of silencing nuclear factor (NF)κB1 mRNA in bone marrow CD34+ cells from patients with rheumatoid arthritis on the viable cell counts and the production of $\beta_2$-microblobulin ($\beta_2$MG). Purified bone marrow CD34+ cells from patients with rheumatoid arthritis were transfected with small interfering RNA (siRNA) for NFκB1 or scrambled sequence control siRNA, after which the cells were further incubated in culture medium with stem cell factor (10 ng/ml), granulocyte-macrophage colony stimulating factor (1 ng/ml) and tumor necrosis factor-α (10 ng/ml) up to 4 weeks with no medium changes. After various periods of incubation (W, weeks), the cells were counted and the quantities of $\beta_2$MG in the culture supernatants were determined by ELISA. This is the same experment as shown in Figure 13. Data are representative of three different experiments.

to the decreased stability of IκBβ mRNA [11]. Since IκB plays an important role in inhibition of translocation of NFκB into the nucleus, the decrease in RelA mRNA might result in enhanced activation of NFκB related genes through upregulation of the translocation of NFκB. It is suggested, therefore, that the decreased expression of RelA mRNA in RA bone marrow CD34+ cells might also contribute to abnormal response to TNF-α.

It is possible that the upregulation of NFκB1 mRNA in bone marrow CD34+ cells might be secondary to the increased levels of TNF-α in the bone marrow. In fact, the treatment of bone marrow CD34+ cells from healthy individuals with TNF-α resulted in the increased expression of NFκB1 mRNA. However, TNF-α also enhanced the expression of mRNAs for NFκB2 and RelA in bone marrow CD34+ cells from healthy individuals. Of note, the expression of RelA mRNA appeared to be rather decreased in RA bone marrow CD34+ cells as mentioned above. Taken together, these data strongly suggest that the enhanced expression of NFκB1 mRNA might not be due simply to the increased levels of TNF-α in the bone marrow. Further studies to explore the mechanism of abnormal expression of NFκB1 mRNA in bone marrow CD34+ cells would be important for delineation of the pathogenesis of RA.

The role of the enhanced expression of NFκB1 mRNA in RA bone marrow CD34+ cells in their abnormal responses to TNF-α was further confirmed by the experiments of selective silencing of NFκB1 mRNA. Reduction of NFκB1 mRNA in RA bone marrow CD34+ cells by transfection of siRNA for NFκB1 markedly suppressed the generation of fibroblast-like cells as well as the production of MMP-1 and VEGF under the influence of TNF-α without affecting the viability or the capacity to produce $\beta_2$MG. These results indicate that upregulation of NFκB1 mRNA expression leads to the enhanced responses of RA bone marrow CD34+ cells to TNF-α. Thus, the enhanced NFκB1 mRNA expression might be a critical defect in RA bone marrow CD34+ cells.

Autologous hematopoietic stem cell transplantation (HSCT) has been used to treat severe RA in limited case reports [12,13]. However, a study with large numbers of patients has disclosed that recurrence of RA is frequent in patients who received autologous HSCT [14,15]. Frequent recurrence after autologous HSCT for RA suggests that abnormalities in bone marrow stem cells might persist after the treatment [16,17]. It is possible that the enhanced expression of NFκB1 mRNA might be closely related with such abnormalities in bone marrow stem cells, although further studies are required to confirm this point. It would also be important to explore whether there might be another transcription factor that could be inhibited without suppressing the differentiation of bone marrow CD34+ cells into fibroblast-like cells in order to confirm the importance of NFκB1 mRNA expression in the pathogenesis of RA.

## Conclusion

The present study has revealed the enhanced expression of NFκB1 mRNA in RA bone marrow CD34+ cells as possible intrinsic abnormalities in bone marrow, resulting in abnormal responses to TNF-α. Further studies to delineate the mechanisms for the abnormal NFκB1 mRNA expression would be important for a complete understanding of the pathogenesis and etiology of RA.

## Competing interests

The authors declare that they have no competing interests.

## Authors' contributions

SH designed the study, and participated in experimental procedures, collection, analysis, and interpretation of data, and manuscript preparation. YM and NC contributed to analysis and interpretation of data. TT, HY, and TO contributed to collection and analysis of data. All authors read and approved the final text before submission of the manuscript.

## Acknowledgements

This work is supported by a grant-in-aidfromthe Health Science Research grant from theMinistry of Health and Welfare of Japan and grants from Aventis Pharma Co., Ltd, Tokyo, and from Eisai Co., Ltd, Tokyo, Japan. The authors wish to thank Tamiko Yanagida, PhD, for her technical assistance.

## References

1. Tak PP: **Examination of the synovium and synovial fluid.** In *Rheumatoid arthritis: Frontiers on pathogenesis and treatment* Edited by: Firestein GS, Panayi GS, Wollheim RA. New York: Oxford University Press; 2000:55-68.
2. Hirohata S, Yanagida T, Nagai T, Sawada T, Nakamura H, Yoshino S, Tomita T, Ochi T: **Induction of fibroblast-like cells from CD34(+) progenitor cells of the bone marrow in rheumatoid arthritis.** *J Leukoc Biol* 2001, **70**:413-421.
3. Müller-Ladner U, Gay RE, Gay S: **Role of nuclear factor kappaB in synovial inflammation.** *Curr Rheumatol Rep* 2002, 4:201-207.
4. Feldmann M, Maini RN: **Anti-TNF alpha therapy of rheumatoid arthritis: what have we learned?** *Annu Rev Immunol* 2001, **19**:163-196.
5. Arnett FC, Edworthy SM, Bloch DA, McShane DJ, Fries JF, Cooper NS, Healey LA, Kaplan SR, Liang MH, Luthra HS, *et al.*: **The American Rheumatism Association 1987 revised criteria for the classification of rheumatoid arthritis.** *Arthritis Rheum* 1988, **31**:315-324.
6. Kawai M, Hirohata S: **Cerebrospinal fluid beta(2)-microglobulin in neuro-Behcet's syndrome.** *J Neurol Sci* 2000, **179**:132-139.
7. Evrin PE, Nilsson K: **Beta 2-microglobulin production in vitro by human hematopoletic, mesenchymal, and epithelial cells.** *J Immunol* 1974, **112**:137-144.
8. Child JA, Kushwaha MR: **Serum beta 2-microglobulin in lymphoproliferative and myeloproliferative diseases.** *Hematol Oncol* 1984, **2**:391-401.
9. Bataille R, Grenier J, Commes T: **In vitro production of beta 2 microglobulin by human myeloma cells.** *Cancer Invest* 1988, **6**:271-277.
10. Park HJ, Lee SH, Son DJ, Oh KW, Kim KH, Song HS, Kim GJ, Oh GT, Yoon do Y, Hong JT: **Antiarthritic effect of bee venom: inhibition of inflammation mediator generation by suppression of NF-κB through interaction with the p50 subunit.** *Arthritis Rheum* 2004, **50**:3504-3515.
11. Beg AA, Sha WC, Bronson RT, Ghosh S, Baltimore D: **Embryonic lethality and liver degeneration in mice lacking the RelA component of NF-κB.** *Nature* 1995, **376**:167-170.
12. Joske DJ: **Autologous bone-marrow transplantation for rheumatoid arthritis.** *Lancet* 1997, **350**:337-338.
13. Durez P, Toungouz M, Schandene L, Lambermont M, Goldman M: **Remission and immune reconstitution after T-cell-depleted stem-cell transplantation for rheumatoid arthritis.** *Lancet* 1998, **352**:881.
14. Snowden JA, Passweg J, Moore JJ, Milliken S, Cannell P, Van Laar J, Verburg R, Szer J, Taylor K, Loske D, *et al.*: **Autologous hemopoietic stem cell transplantation in severe rheumatoid arthritis: a report from the EBMT and ABMTR.** *J Rheumatol* 2004, **31**:482-488.
15. Bingham SJ, Moore JJ: **Stem cell transplantation for autoimmune disorders. Rheumatoid arthritis.** *Best Pract Res Clin Haematol* 2004, **17**:263-276.
16. Papadaki HA, Kritikos HD, Gemetzi C, Koutala H, Marsh JCW, Boumpas DT, Eliopoulos GD: **Bone marrow progenitor cell reserve and function and stromal cell function are defective in rheumatoid arthritis: evidence for a tumor necrosis factor alpha-mediated effect.** *Blood* 2002, **99**:1610-1619.
17. Porta C, Caporali R, Epis O, Ramaioli I, Invernizzi R, Rovati B, Comolli G, Danova M, Montecucco C: **Impaired bone marrow hematopoietic progenitor cell function in rheumatoid arthritis patients candidated to autologous hematopoietic stem cell transplantation.** *Bone Marrow Transplant* 2004, **33**:721-728.

# Dual Hydroxyapatite Composite With Porous and Solid Parts: Experimental Study Using Canine Lumbar Interbody Fusion Model

Takashi Kaito, Yoshihiro Mukai, Masataka Nishikawa, Wataru Ando, Hideki Yoshikawa, Akira Myoui

Department of Orthopaedics, Osaka University Graduate School of Medicine, 2–2 Yamadaoka, Suita, Osaka 565-0871, Japan

*Received 23 March 2005; revised 30 August 200; accepted 12 October 2005*
*Published online 30 January 2006 in Wiley InterScience (www.interscience.wiley.com). DOI: 10.1002/jbm.b.30498*

**Abstract:** Hydroxyapatite (HA) has been evaluated for use in a variety of applications in bone reconstruction surgery because of its high affinity with host bone and biocompatibility. However, because of the difficulty in combining porosity (for bone ingrowth) and strength in HA, it is generally considered inappropriate to use HA for high-load applications such as spinal interbody fusion. In the present study, we constructed a HA implant for spinal interbody fusion, composed of a dual HA composite (DHC) that combines two HA materials with different porosities: HA with 75% porosity, for bone ingrowth; and HA with 0% porosity, for load bearing. We used a canine lumbar interbody fusion model to evaluate bone conduction of the implant and its efficacy for bony fusion. Six months after the operation, DHC exhibited almost the same efficacy for bony fusion as iliac bone grafts. Moreover, pores of the porous part of the DHC were completely filled with newly formed bone and bone marrow cells. The present findings indicate that DHC is suitable for use as an implant material for spinal interbody fusion as a substitute for iliac bone grafts, which could eliminate the disadvantages associated with autograft harvesting. © 2006 Wiley Periodicals, Inc. J Biomed Mater Res Part B: Appl Biomater 78B: 378–384, 2006

Keywords: hydroxyapatite; spinal fusion; composite

## INTRODUCTION

When instability of the spine causes persistent local pain or neurological impairment, it is often treated by fusion of the affected vertebral motor segments with autologous bone graft by itself or in combination with carbon or titanium cage.[1–3] So at this point, autologous bone graft from the iliac crest is the gold standard material for spinal fusion, despite disadvantages such as limited supplies of suitable bone, cosmetic damage at the donor site, and persistence of pain, nerve damage, and fracture. Allografting is not associated with donor site problems, but it involves risks of disease transmission and immunological reaction.[4] Hydroxyapatite (HA) implants are an attractive alternative to bone grafts for use in spinal arthrodesis. Porous ceramics provide a three-dimensional (3D) scaffold for the osteoconductive latticework that is necessary for host ingrowth. HA can chemically bond with host bone, and studies clearly indicate that it is a biocompatible material.[5,6] However, the difficulty in striking a balance between porosity (for bone ingrowth) and strength has prevented widespread use of HA as an implant material for use in spinal interbody fusion.[7–11] To address this problem, we synthesized a dual HA composite (DHC) consisting of a core of HA with 75% porosity (for bone ingrowth) surrounded by solid HA with 0% porosity (for load bearing). The porous part of the composite is a material that we previously reported as interconnected porous calcium HA ceramic (IP-CHA). This porous material is synthesized using a unique "foam–gel" technique that produces its distinctive, uniform porous structure.[12]

In the present study, we used an anterior interbody fusion model of the canine lumbar spine to assess the efficacy of DHC as a spinal interbody fusion implant, compared with iliac bone grafts, in terms of bony fusion.

## MATERIALS AND METHODS

### Design of Implants

The implants were designed to fit the canine intervertebral space (Figure 1). Also, a stainless steel plate, with four screw holes for internal fixation, was designed to fit the canine spine (Figure 1).

### Preparation of Implants

Hexagonal prisms of DHC were obtained from Toshiba Ceramics (Kanagawa, Japan) (Figure 1). The DHC consisted of

*Correspondence to:* T. Kaito (e-mail: t-kaito@leto.conct.ne.jp)
Contract grant sponsor: Ministry of Health, Labor and Welfare, Japan
Contract grant sponsor: Ministry of Education, Culture, Sports, Science and Technology, Japan; contract grant number: 15209050

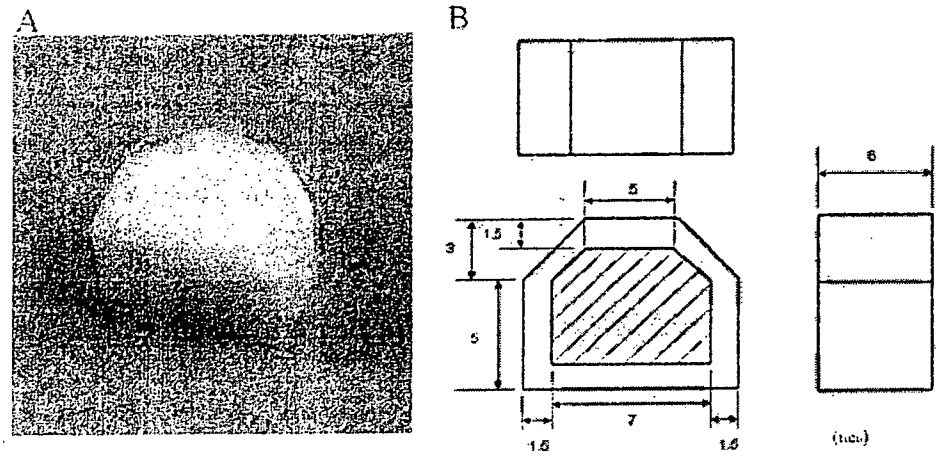


**Figure 1.** Macroscopic view (A) and dimensions (B) of dual hydroxyapatite composite (DHC) implant for canine intervertebral body fusion. Hatched area represents porous part (75% porosity).

two forms of HA with different porosity. A porous HA ceramic core with 75% porosity was surrounded by a solid HA ceramic with 0% porosity. The material comprising the porous HA ceramic core was IP-CHA, which has a uniform interconnected porous structure with an average interconnection channel diameter of 40 $\mu$m. Theoretically, more than 90% of the pores are connected to each other by channels with a diameter greater than 10 $\mu$m, allowing tissue to spread from pore to pore.[12] Briefly, the method used to produce DHC is as follows:

1. *Preparation of Porous HA Ceramic*:

A slurry containing HA (60 wt %) and a crosslinking substrate (polyethyleneimine, 40 wt %) was mixed with a foaming agent (polyoxyethylene lauryl ether, 1 wt %). Then, the slurry was gelatinized by adding another crosslinking agent (poly-functional epoxy compound). After the gelatinization, a hexagonal prism was carved out of the porous gel.

2. *Preparation of Solid HA Ceramic:*

A piece of the carved porous gel was placed in the center of a hexagonal mold with larger dimensions. A slurry with the same composition as the above-mentioned slurry, but lacking the foaming agent, was mixed with the gelatinization agent and poured into the mold so that it surrounds the porous gel. The nonfoaming slurry infiltrated the surface layer of the porous part and then hardened to form the solid HA ceramic, such that the solid and porous parts of the composite were tightly bound together. Then, the dual composite was removed from the mold, dried, and sintered at 1200°C.

### Mechanical Compression Test

Compression tests were performed using AUTOGRAPH AG-10KNI (Shimadzu Corp., Kyoto, Japan), with a compression speed of 1 mm/min. Compression load was applied separately to the porous and solid parts, and the compressive strength was determined. Maximum breaking load of the hexagonal DHC implant was measured by applying a vertical compressive load to the specimen, across the hexagonal surface plane ($N = 4$). All data were expressed as the average value ± standard error.

### Animal Experiment

Eight adult, female, pure-bred beagles aged ~1.5 years and weighing 12–14 kg underwent surgical opening of a left retroperitoneal approach to the lumbar spine. The surgery was performed using general anesthesia, aseptic conditions, and perioperative antibiotics. The segmental vessels of L2 and L3 were coagulated and transected to expose the bodies of L2 and L3. Then, the center portion of the intervertebral disc was identified and evacuated including the adjacent endplates of L2 and L3, using steel and diamond burrs to expose bleeding subchondral bone. The defect size was adjusted using a metal trial tool that was the same size as the implant. We then performed one-level arthrodesis by placing an iliac bone graft (IBG group) or a DHC graft (DHC group) in the defect. In all animals, internal fixation was achieved using a plate and four cortical screws (Ø, 4.0 mm) (Figure 2). The animals were allowed unrestricted activity after the operative procedure, and were kept in accordance with our institutional guidelines for care and use of laboratory animals. Dogs were killed by overdose anesthesia, and the spine segment from L1 to L4 was harvested 6 months after operation. Then, the internal fixators were removed. All procedures involving animals were approved by the Animal Care and Use Committee of Shin Nippon Biomedical Laboratories and performed in accordance with standards published by the National Research Council.

### Radiographic Examination

All harvested tissues were fixed with 10% neutral formalin, and were then radiographed with a soft X-ray apparatus (M-60, SOFTEX Corp., Ebina, Japan) and micro-focus CT scanning apparatus (SMX-100CT, SHIMADZU, Kyoto, Japan). On radiographs and CT images, fusion was defined as

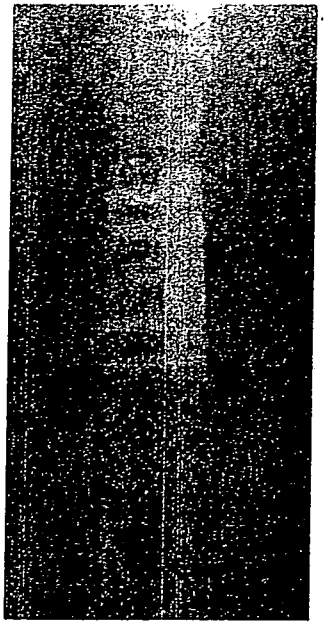

**Figure 2.** Postoperative A-P radiographic view of canine lumbar spine.

a continuous trabecular bone bridge across the inner part of the implant, with no obvious interruption by a radiolucent line.

### Histological Evaluation

All tissue samples harvested together with the neighboring vertebral bone from each group were demineralized with 50% formic acid and 10% sodium citrate, dehydrated through an ethanol series and embedded in paraffin wax. Sections (thickness, 5 $\mu$m) were cut, stained with hematoxylin and eosin, and examined under a light microscope.

Bony union was quantified by calculating % length of bony fusion, which is judged by bridging trabecular bone between host bone and porous part of DHC or iliac bone graft histomorphometrically. Solid parts of DHC were evaluated independently. The number of invaded blood vessels was quantified by counting vessels in arbitrary 10 fields of histological sections of porous part of DHC or IBG.

### Statistical Analysis

Compressive strength was compared between the porous and solid parts of the DHC implants, using Student's $t$-test. $p < 0.05$ was considered significant.

## RESULTS

### Mechanical Compression Test

The compressive strength of the porous (inner) part of the DHC was 12.6 ± 0.4 Mpa, which is comparable to the compressive strength of cancellous bone. In contrast, the compressive strength of the solid (outer) part was 571.8 ± 66.7 Mpa, which is equal to or greater than the compressive strength of cortical bone. The strength of the outer part of the composite was more than 50-fold greater than that of the inner part, and the difference was statistically significant. The breaking load of the DHC implant was 9.6 ± 0.3 kN.

### Radiographic Evaluation

In the DHC group, the radiolucent line between the implant and host bone faded with time, but on the cranial side of the implant, the radiodensity between the implant and host bone remained low, compared with other boundaries. None of the implants were found to have collapsed. In the IBG group, all caudal and cranial junctions appeared to have fused with host bone on radiographs. In both groups, the height of the intervertebral space remained constant throughout the follow-up period (Figure 3, Table I).

### Micro-Focus CT Evaluation

In the DHC group, the plain radiographic findings correlated well with the CT findings. In all caudal junctions of the DHC group, trabecular bone extended from the host bone and spread to the porous part of the composites. However, on the cranial side of the implant, none of the specimens contained bridging trabecular bone between the implant and host bone. One specimen had a nondisplaced crack line through the inner part of the implant [Figure 4(A-4)], and another specimen had a small crack at the cranial edge of the implant [Figure 4(A-3)].

In the IBG group, 5 of the 8 junctions were bony fused, and the remaining 3 junctions (which were initially judged to be bony fused, based on X-ray findings) were classified as nonbony fused junctions, based on micro-focus CT findings. All of the nonbony fused junctions were on the cranial side of the graft bone (Figure 4, Table I).

### Histology

The macroscopic appearance of the histological sections was consistent with the findings of micro-focus CT. In the DHC group, all caudal junctions were found to contain trabecular bone and blood vessels that had spread from host bone into the porous part of the implants [Figure 5(A1–A4,c)]. At the center of each implant, nearly all pores were completely filled with trabecular bone and hematopoietic marrow, including the region that originally contained the vertebral disc [Figure 5(b)]. On the cranial side of the implant, a good portion of the initial gap between the implant and host bone was filled with a fibrocartilage tissue, rather than mineralized bone matrix [Figure 5(a)].

In the IBG group, the caudal side of each graft was bony fused in large part, and it was impossible to identify a boundary between host and graft bone.

The cranial side of 1 of the 4 grafts was mostly bony fused, but in the other 3 samples, there was a thin layer of cartilage tissue between host and graft bone [Figure 5(B)]. Solid part

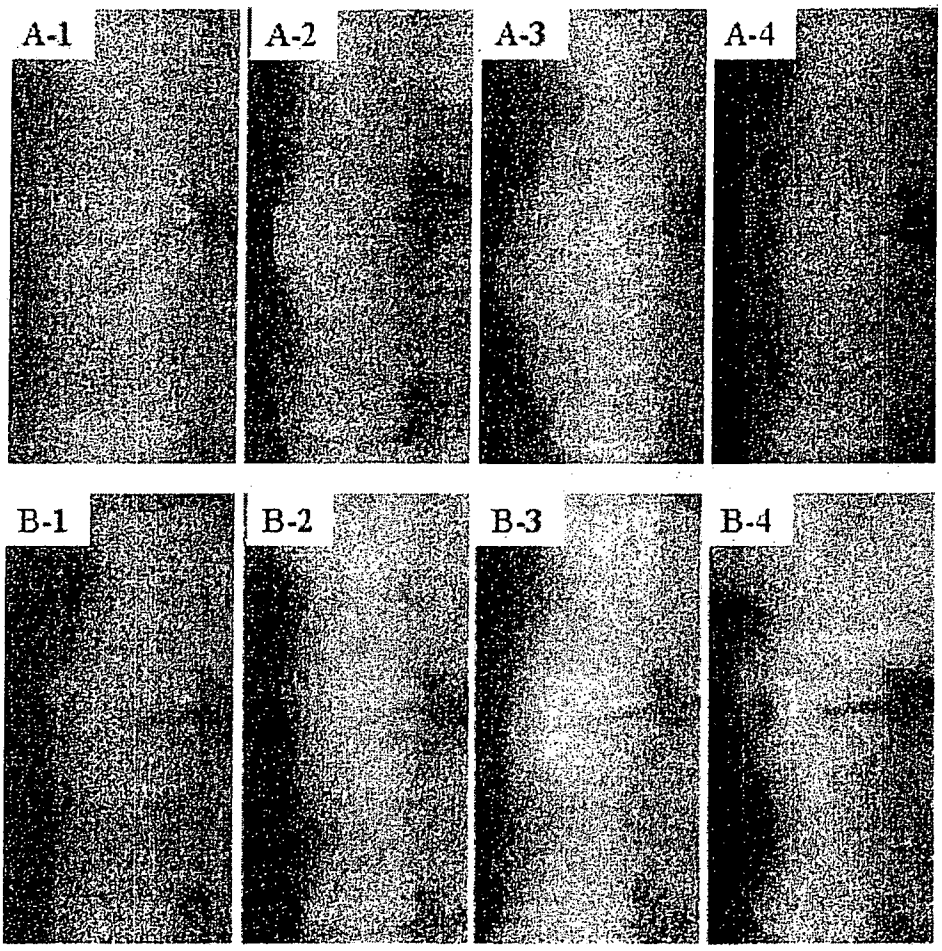


**Figure 3.** Soft X-ray radiographs. DHC group 6 months after operation (A1–A4). IBG group 6 months after implantation (B1–B4). In both groups, radiopaque shadows were observed at caudal junctional sites. Cranial junctions of DHC group had lower radiodensity than other boundaries between DHC and host bone (A1–A4). Both cranial and caudal sides of all IBG specimens appeared to be radiographically fused (B1–B4).

of the DHC showed by far lower fusion rate when compared with porous part of DHC and IBG.

There was no difference in the invasion of the material by blood vessels between IBG and DHC group.(Figures 6 and 7, Table II).

## DISCUSSION

Because of problems including graft extrusion and collapse in animal models and clinical study, HA spinal interbody fusion implants are generally considered unsuitable for clinical applications, despite their high affinity with host bone and their biocompatibility.[4,13,14] Among currently existing porous HA-based bone substitutes, IP-CHA and coralline HA have highly interconnected porous structure with average interconnection channel diameter of 40–60 $\mu$m. Those materials have been reported to show excellent bone ingrowth in the materials but their initial compressive strengths are no more than 12 MPa, which is far less than human cortical bone. A porous HA bone substitute with lowest porosity (40%) accomplished the greatest compressive strength of 60 MPa at the sacrifice of osteoconduction but the strength is not still comparable to cortical bone. Our novel dual HA implant (DHC) has well-organized, interconnected, highly porous structure in the porous part and durability under high loads at the same time. In our development of a HA implant for use in spinal interbody fusion, rather than use a material of homogenous composition, we created a composite HA material consisting of two parts with different porosities to produce an implant that combines strength with bone conduction. The outer solid part of the composite (0% porosity), which can chemically bond

**TABLE I. Summary of Radiographic Evaluation**

| | X-ray Evaluation | | Micro-Focus CT Evaluation | | | |
|---|---|---|---|---|---|---|
| | | | | | Crack | |
| Groups | Fusion | Fusion Rate (%) | Fusion | Fusion Rate (%) | Partial | Whole Length |
| DHC | 4/8 | 50 | 4/8 | 50 | 1/4 | 1/4 |
| IBG | 8/8 | 100 | 5/8 | 62.5 | | |

Each implants or grafts has two junctions between host bone. These data shows union junctions per total junctions (ref. 11).

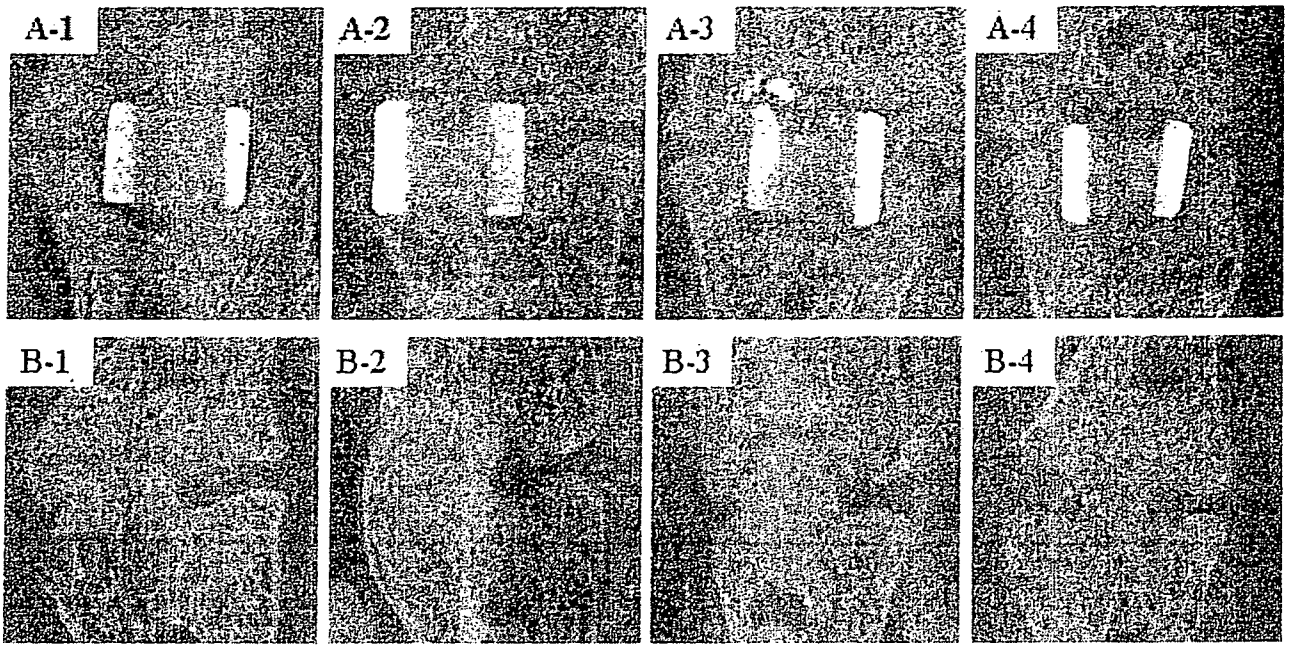


**Figure 4.** Sagittal reconstruction image of operated spine, based on micro-focus CT data. DHC group 6 months after operation (A1–A4). IBG group 6 months after implantation (B1–B4). In both groups, the caudal side of all junctions was bony fused (A1–A4, B1–B4). Only one sample of the IBG group exhibited osseous union at the cranial junction (B2). At other cranial junctions of both groups, we did not observe bridging trabecular bone between the implant and host bone (A1–A4, B1, B3, B4).

with host bone, is mainly responsible for load bearing, which is the role normally played by cortical bone. The inner porous part of the composite (75% porosity) assumes the role of scaffold to facilitate integration with host bone and thus further strengthen the repair structure.

In the present study, the junctional bony union rate of DHC was 50% and was less than that of the iliac bone grafts. However, most of the junctional gap without bony union was filled with fibro-cartilageous tissue and seemed to be stabilized. Also, only one specimen from the DHC group exhibited a nondisplaced crack spanning the entire length of the implant. None of the DHC implants exhibited axial collapse at any time during the 6-month experimental period. Implant fragmentation is one of the most frequent complications of porous HA implants for intervertebral fusion. DHC seems to have less fragmentation rate but further study with large number is needed to clarify the rate of complications and the advantage of DHC.

Independent of the junctional bony union, the inner part of DHC exhibited excellent bone ingrowth. By covering the porous HA with nonporous HA, the 3D structure of the porous part was preserved throughout the bone conduction process, providing an excellent scaffold for bone ingrowth. The interconnected highly porous structure of IP-CHA, which has an average interconnection diameter of 40 $\mu$m, allows efficient migration of bone-producing cells from pore to pore as well as invasion by vascular vessels, which is essential for new bone formation. The present findings help clarify the importance of a stable 3D scaffold for bone ingrowth. The use of a diamond burr in the present procedure

**TABLE II. Summary of Histological Evaluation**

| | Junctions[a] | Tissue Conduction | | | |
|---|---|---|---|---|---|
| | | Vessel[b] | Bone[c] | | |
| Groups | Average Bony-Fusion Rate (%) | Average Number of the Blood Vessels | Cranial | Center | Caudal |
| Porous part of DHC | 48 | 215 | 4/4 | 4/4 | 4/4 |
| IBG | 53 | 193 | | | |
| Solid part of DHC | 19 | | | | |

[a] Each implants or grafts has two junctions between host bone. These data shows mean bony union length per total junctional length ($N$ = 4).
[b] Total number of invaded blood vessels into porous part of DHC and IBG in arbitrary 10 fields ($N$ = 4).
[c] Porous part of DHC was divided into three parts. These data shows bone conducted parts per total DHC implants (ref. 7).

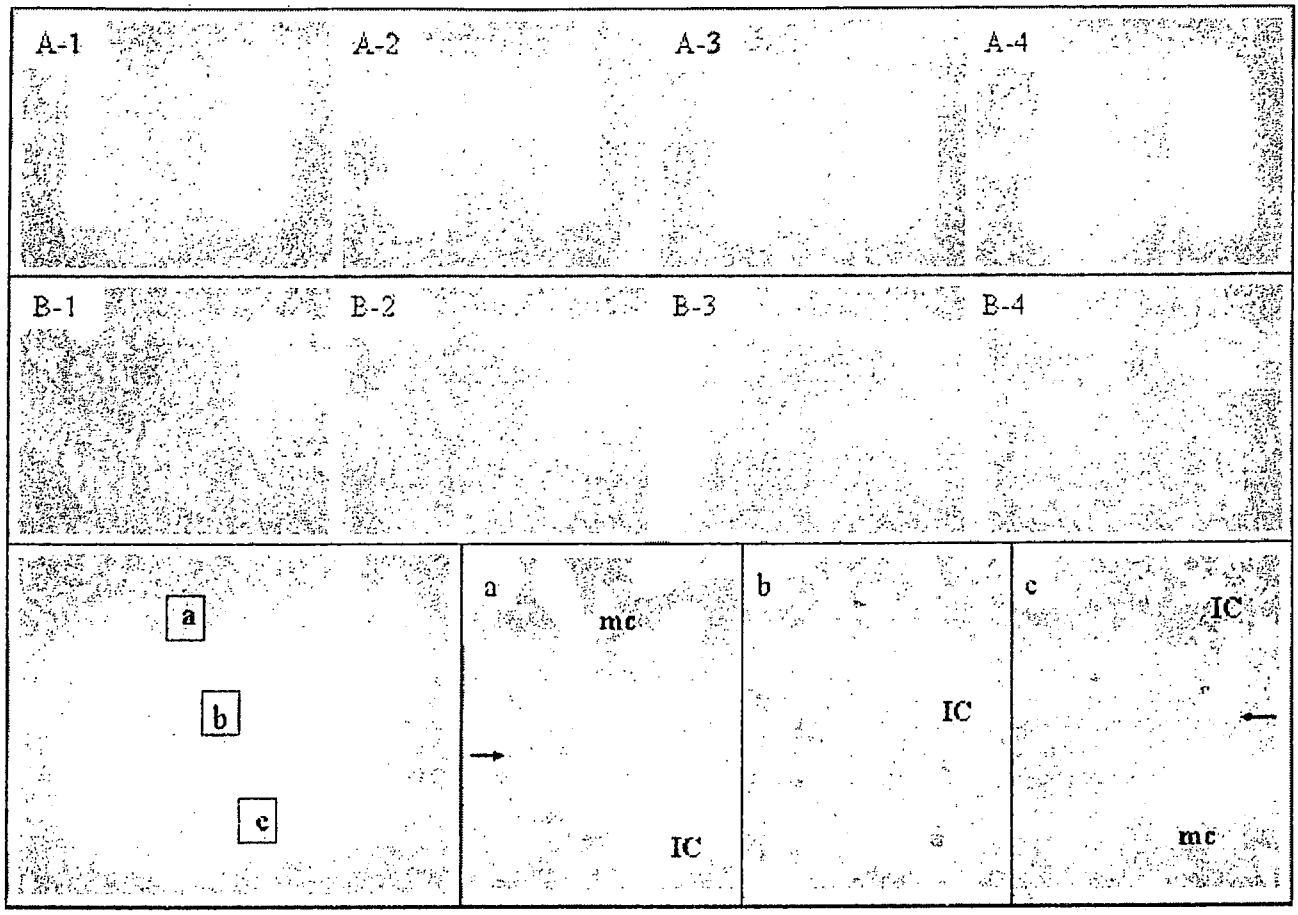


**Figure 5.** Low-power photomicrographs of operated spines: DHC (A1–A4); and IBG (B1–B4). High-power photomicrographs of DHC group 6 months after operation (a–c). At the cranial side of the implant, we did not observe continuous mineralized trabecular bone between host bone and DHC (a). Almost all pores in the DHC were evenly filled with trabecular bone and hematopoietic marrow (b). At the caudal junction, trabecular bone infiltrated the porous part of DHC, and the gaps were filled with mineralized trabecular bone (c). mc, marrow cavity; IC, IP-CHA. Arrows indicate implant end (magnification: ×40).

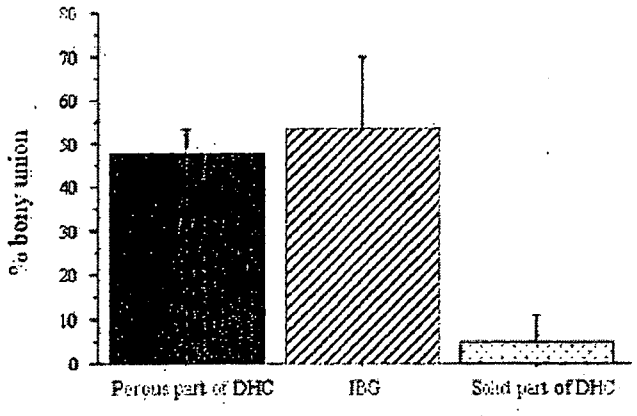


**Figure 6.** Bone union rates of porous part of DHC, IBG, and solid part of DHC were measured histomorphometrically. Each data bar represents an average and standard deviation ($N$ = 5).

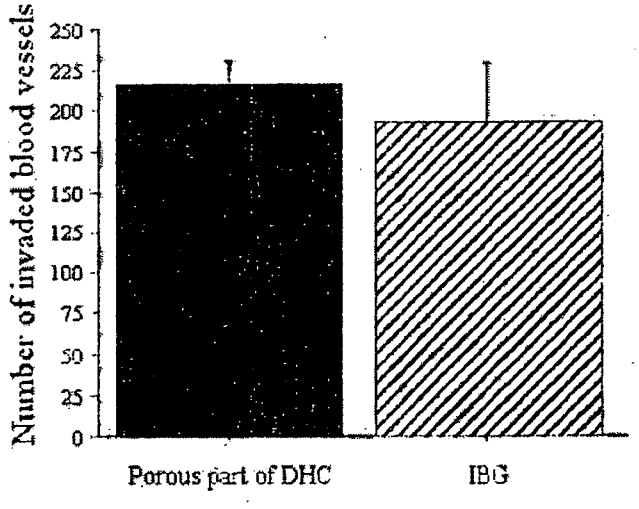


**Figure 7.** The number of invaded blood vessels were counted in arbitrary 10 fields of histological sections of porous part of DHC or IBG. Each data bar represents an average and standard deviation ($N$ = 5).

generates frictional heat, which may have an adverse affect on cell protection and congruency between host bone and implant, and this may inhibit junctional bony union. In terms of their role as scaffolding, interconnected HA and autogenous bone have nearly identical characteristics. In the present animal experiment, the internal fixation at the operative site consisted of a single plate, and was not rigid; no external fixation was applied; and animals were allowed complete freedom of movement immediately after the surgery. However, none of the animals experienced major implant-related complications such as implant collapse, displacement, dislocation, or spinal palsy. Although we observed minor cracks (which did not affect the stability of the implanted sites), our results suggest that DHC has sufficient compressive strength to endure typical intervertebral mechanical loads. The high compressive strength of DHC and the excellent bone ingrowth into the porous part of DHC observed in the present experiment indicate that DHC is highly suitable as a spacing implant material for intervertebral fusion.

However, autogenous bone has the advantage of containing bone-producing cells and several cytokines that contribute to bone induction. HA is an osteoconductive material, but it must be combined with bone-growth-inducing cytokines or bone-producing cells before it can provide results comparable to those of autogenous bone grafts. As we reported previously, porous HA can exhibit good bone-growth-inducing characteristics when it is combined with a cytokine delivery system[15–20] or bone-producing cells such as mesenchymal stem cells. DHC supplemented with those cytokines and cells would be an excellent interbody fusion biomaterial, due to the combination of bone-growth-inducing characteristics and mechanical strength, and it would be a viable substitute for autografts.

## CONCLUSIONS

The present findings demonstrate that DHC produces bony fusion that is comparable to that of autogenous iliac bone graft, with strength that is sufficient to withstand normal compressive loads. Further improvement of this material, including incorporation of bone-growth-inducing agents, will increase its usefulness for clinical applications.

We thank Toshiba Ceramics Co., Ltd., for kindly donating implants.

## REFERENCES

1. Buttermann GR, Glazer PA, Bradford DS. The use of bone allografts in the spine. Clin Orthop Relat Res 1996;324:75–85.
2. Malloy KM, Hilibrand AS. Autograft versus allograft in degenerative cervical disease. Clin Orthop Relat Res 2002;394:27–38.
3. Blumenthal SL, Ohnmeiss DD. Intervertebral cages for degenerative spinal diseases. Spine J 2003;3:301–309.
4. Goldberg VM. Natural history of autografts and allografts. In: Older J, editor. Bone Implant Grafting. London: Springer-Verlag; 1992. p 9–12.
5. Bucholz RW, Carlton A, Holmes RE. Hydroxyapatite and tricalcium phosphate boe graft substitutes. Orthop Clin North Am 1987;18:323–334.
6. Flatley TJ, Lynch KL, Benson M. Tissue response to implant s of calcium phosphate ceramic in the rabbit spine. Clin Orthop 1983;179:246–252.
7. Ylinen P, Kinnunen J, Laasonen EM, Lamminen A, Vainionpaa S, Raekollio M, Rokkanen P. Lumbar spine interbody fusion with reinforced hydroxyapatite implants. Arch Orthop Trauma Surg 1991;110:250–256.
8. Jeffrey MS. Use of hydroxyapatite in spine surgery. Eur Spine J 2001;10:S197–S204.
9. Emery SE, Fuller DA, Stevenson S. Ceramic anterior spinal fusion. Biologic and biomechanical comparison in a canine model. Spine 1996;21:2713–2719.
10. Lu WW, Zhao F, Luk KDK, Yin YJ, Cheung KMC, Cheng GX, Yao KD, Leong JCY. Controllable porosity hydroxyapatite ceramics as spine cage: Fabrication and properties evaluation. J Mater Sci Mater Med 2003;14:1039–1046.
11. Frank AP, Dennis JM, James PH, Narayon Y, Kark WD, John MR, Brian C. Fusion rate and biomechanical stiffness of hydroxylapatite versus autogenous bone grafts for anterior discectomy. Spine 1994;19:2524–2528.
12. Tamai N, Myoui A, Tomita T, Nakase T, Tanaka J, Ochi T, Yoshikawa H. Novel Hydroxyapatite ceramics with an interconnective porpus structure exhibit superior osteoconduction in vivo. J Biomed Mater Res 2002;59:110–117.
13. Ito M, Abumi K, Shono Y, Kotani Y, Minami A, Kaneda K. Complications related to hydroxyapatite vertebral spacer in anterior cervical spine surgery. Spine 2002;27:428–431.
14. McConnell JR, Freeman BJ, Debnath UK, Grevitt MP, Prince HG, Webb JK. A prospective randomized comparison of coralline hydroxyapatite with autograft in cervical interbody fusion. Spine 2003;28:317–323.
15. Saito N, Takaoka K. New synthetic biodegradable polymers as BMP carriers for bone tissue engineering. Biomaterials 2003; 24:2287–2293.
16. Miyamoto S, Takaoka K, Okada T, Yoshikawa H, Hashimoto J, Suzuki S, Ono K. Evaluation of polylactic acid homopolymers as carriers for bone morphogenetic protein. Clin Orthop 1992; 278:274–285.
17. Miyamoto S, Takaoka K, Okada T, Yoshikawa H, Hashimoto J, Suzuki S, Ono K. Polylactic acid–polyethylene glycol block copolymer: A new biodegradable synthetic carrier for bone morphogenetic protein. Clin Orthop 1993;294:333–343.
18. Saito N, Okada T, Horiuchi H, Murakami N, Takahashi J, Nawata M, Ota H, Nozaki K, Takaoka K. A biodegradable polymer as a cytokine delivery system for inducing bone formation. Nat Biotechnol 2001;19:332–335.
19. Kaito T, Myoui A, Takaoka K, Saito N, Nishikawa M, Tamai N, Ohgushi H, Yoshikawa H. Potentiation of the activity of bone morphogenetic protein-2 in bone regeneration by a PLA-PEG/hydroxyapatite composite. Biomaterials 2005;26:73–79.
20. Nishikawa M, Myoui A, Ohgushi H, Ikeuchi M, Tamai N, Yoshikawa H. Bone tissue engineering using novel interconnected porous hydroxyapatite ceramics combined with marrow mesenchymal cells: Quantitative and three-dimensional image analysis. Cell Transplant 2004;13:367–376.

Vol 443|26 October 2006|doi:10.1038/nature05245

LETTERS

# Chronic polyarthritis caused by mammalian DNA that escapes from degradation in macrophages

Kohki Kawane[1,3,4], Mayumi Ohtani[1,4], Keiko Miwa[1,4]†, Takuji Kizawa[2], Yoshiyuki Kanbara[5], Yoshichika Yoshioka[5], Hideki Yoshikawa[2] & Shigekazu Nagata[1,3,4]

**A large amount of chromosomal DNA is degraded during programmed cell death and definitive erythropoiesis[1]. DNase II is an enzyme that digests the chromosomal DNA of apoptotic cells and nuclei expelled from erythroid precursor cells after macrophages have engulfed them[1,2]. Here we show that *DNase II*$^{-/-}$ *IFN-IR*$^{-/-}$ mice and mice with an induced deletion of the *DNase II* gene develop a chronic polyarthritis resembling human rheumatoid arthritis. A set of cytokine genes was strongly activated in the affected joints of these mice, and their serum contained high levels of anti-cyclic citrullinated peptide antibody, rheumatoid factor and matrix metalloproteinase-3. Early in the pathogenesis, expression of the gene encoding tumour necrosis factor (TNF)-α was upregulated in the bone marrow, and administration of anti-TNF-α antibody prevented the development of arthritis. These results indicate that if macrophages cannot degrade mammalian DNA from erythroid precursors and apoptotic cells, they produce TNF-α, which activates synovial cells to produce various cytokines, leading to the development of chronic polyarthritis.**

*DNase II*$^{-/-}$ mice die as embryos as a result of the constitutive production of interferon (IFN)-β[3,4], and this lethality can be rescued by a deficiency of the *IFN-IR* gene[5]. *DNase II*$^{-/-}$*IFN-IR*$^{-/-}$ mice were born normal, at a slightly reduced mendelian ratio, but they developed polyarthritis as they aged (see below). To examine whether mice carrying a single deletion in *DNase II* gene develop arthritis, we introduced a floxed allele into the *DNase II* gene (Supplementary Fig. S1). These mice were crossed with *Mx1-Cre* mice, which carry the *Cre* gene under the control of *Mx1*, an IFN-inducible promoter[6], and *DNase II*$^{flox/-}$*Mx1-Cre*$^{T}$ mice were established. When these mice were treated with poly(I)•poly(C) to induce IFN, the floxed region of *DNase II* gene was deleted within 2 months in the spleen (Supplementary Fig. S2), and DNase II messenger RNA was undetectable in the spleen and bone marrow (Supplementary Fig. S3). Hereafter we refer to the poly(I)•poly(C)-treated *DNase II*$^{flox/-}$ mice as *DNase II*$^{Δ/-}$ mice.

The inactivation of the *DNase II* gene in adult mice was not lethal. However, *DNase II*$^{Δ/-}$, but not poly(I)•poly(C)-treated

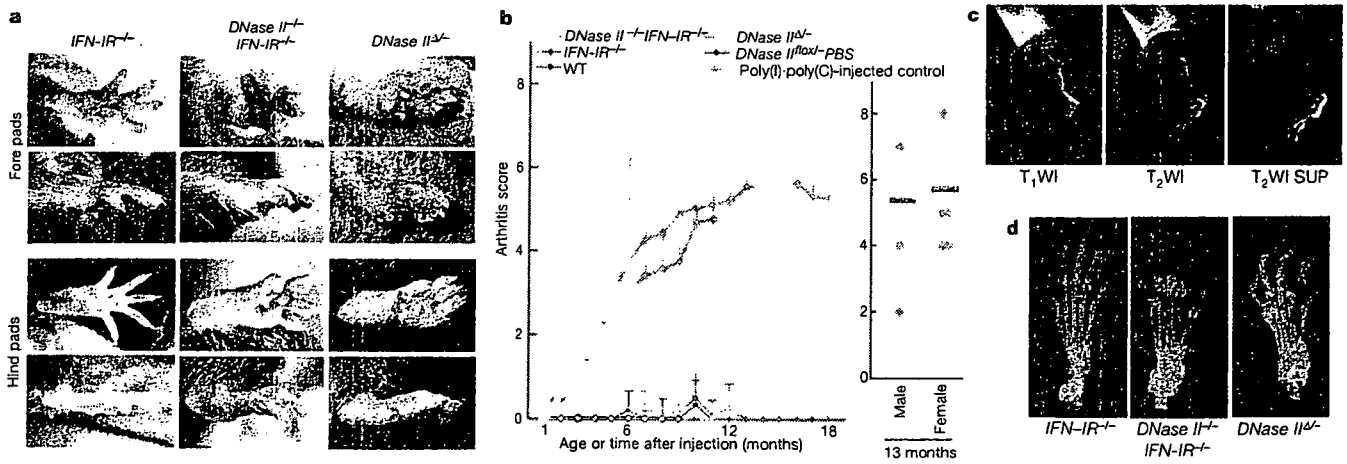


**Figure 1 | Arthritis in *DNase II*$^{-/-}$*IFN-IR*$^{-/-}$ and *DNase II*$^{Δ/-}$ mice.** **a**, Joint swelling of *DNase II*$^{-/-}$*IFN-IR*$^{-/-}$ at the age of 12.5 months, and *DNase II*$^{Δ/-}$ 8–10 months after treatment with poly(I)•poly(C). Joints of *IFN-IR*$^{-/-}$ mice are shown as control. **b**, Left, joints of wild-type ($n$ = 3–4), *IFN-IR*$^{-/-}$ ($n$ = 5–8) and *DNase II*$^{-/-}$*IFN-IR*$^{-/-}$ ($n$ = 9–10) mice were examined at the indicated ages. *DNase II*$^{flox/-}$ ($n$ = 8–10) and *DNase II*$^{flox/+}$ ($n$ = 11–15) littermates were given poly(I)•poly(C) or PBS ($n$ = 5), and examined after the indicated periods. The arthritis scores are plotted as means and s.d. Right, the scores of 13-month-old *DNase II*$^{-/-}$*IFN-IR*$^{-/-}$ are plotted according to sex. The average values are indicated by horizontal red lines. **c**, MRI of the hindlimb of a 15-month-old *DNase II*$^{-/-}$*IFN-IR*$^{-/-}$ mouse. $T_1$-weighted images ($T_1$WI), $T_2$-weighted images ($T_2$WI) and $T_2$-weighted images with fat suppression ($T_2$WI SUP) are shown. **d**, Radiographic examination of the hindlimbs from a 15.5-month-old *DNase II*$^{-/-}$*IFN-IR*$^{-/-}$ and a *DNase II*$^{Δ/-}$ mouse 10 months after treatment with poly(I)•poly(C).

[1]Department of Genetics and [2]Department of Orthopaedics, Osaka University Medical School, Osaka 565-0871, Japan. [3]Laboratory of Genetics, Integrated Biology Laboratories, Graduate School of Frontier Biosciences, Osaka University, Osaka 565-0871, Japan. [4]Solution Oriented Research for Science and Technology, Japan Science and Technology Corporation, Osaka 565-0871, Japan. [5]High Field Magnetic Resonance Imaging Research Institute, Advanced Medical Science Research Centre, Iwate Medical University, Takizawa 020-0173, Japan. †Present address: Laboratory of Cell Lineage Modulation, RIKEN Kobe Institute, Kobe 650-0047, Japan.

*DNase II*$^{flox/+}$ mice, developed chronic polyarthritis in a time-dependent manner (Fig. 1). In *DNase II*$^{-/-}$*IFN-IR*$^{-/-}$ mice at 2–3 months of age or in *DNase II*$^{flox/-}$ mice 2–3 months after treatment with poly(I)•poly(C), forelimbs and hindlimbs began to swell. Swelling affected first the digit, then the foot, and finally the wrist and ankles. Individual mutant mice followed a significantly different time course, but all the mice were eventually affected. As swelling progressed, the mutant mice gradually lost their grasp strength, and their joints became deformed. There was no clear difference between male and female mice in disease development (Fig. 1b). Magnetic resonance imaging (MRI) of the affected joints showed high-intensity signals on the $T_2$-weighted image around tarsal bones and phalanges (Fig. 1c). These high-intensity regions were also observed on the fat-suppressed $T_2$-weighted image, indicating that the joints suffered massive inflammation. Radiographic examination revealed destruction, erosion, and deformity of the subchondral bones (Fig. 1d).

Histology of the swollen joints from both *DNase II*$^{-/-}$*IFN-IR*$^{-/-}$ and *DNase II*$^{\Delta/-}$ mice showed severe synovitis with villus proliferation accompanied by pannus formation (Fig. 2a). Pannus filled the joint cavity, eroded cartilage, destroyed bones, and occasionally penetrated the bone marrow. Pannus was dominated by macrophages carrying the CD68 antigen, among which tartrate-resistant acid phosphatase (TRAP)-positive osteoclasts were at the leading edge. Infiltration of subsynovial tissues by T cells and neutrophils was also observed (Fig. 2a, and data not shown). The abnormal inflammation was limited to the joints, and no apparent disorder was found in the skin, liver, salivary glands, gut or blood vessels of most of the mice.

A set of cytokines and chemokines is known to be highly expressed in the joints of human patients with rheumatoid arthritis[7–9]. Real-time polymerase chain reaction (PCR) analysis indicated that levels of mRNA for TNF-α, interleukin (IL)-1β, IL-6, IL-10, IFN-β and IFN-γ in the affected joints of *DNase II*$^{-/-}$*IFN-IR*$^{-/-}$ and *DNase II*$^{\Delta/-}$ mice were 5–100-fold those in control mice (Fig. 2b). The level of mRNA for IL-18 in the joints of *DNase II*$^{-/-}$ mice was comparable to that in control mice. However, the level of IL-18 protein was very high in the serum of *DNase II*$^{-/-}$*IFN-IR*$^{-/-}$ and *DNase II*$^{\Delta/-}$ mice (Fig. 2c), indicating that the expression of IL-18 might be regulated post-transcriptionally. Matrix metalloproteinase (MMP)-3 is produced by synovial cells of human patients with rheumatoid arthritis and seems to be involved in the degradation of the extracellular matrix[10]. Accordingly, the level of the mRNA for MMP-3 in the joints of *DNase II*$^{-/-}$*IFN-IR*$^{-/-}$ and *DNase II*$^{\Delta/-}$ mice was more than 25-fold that in control mice (Fig. 2b), and its protein level in the serum was also 2–3-fold higher in the mutant mice (Fig. 2c). Anti-cyclic citrullinated peptide (CCP) antibody,

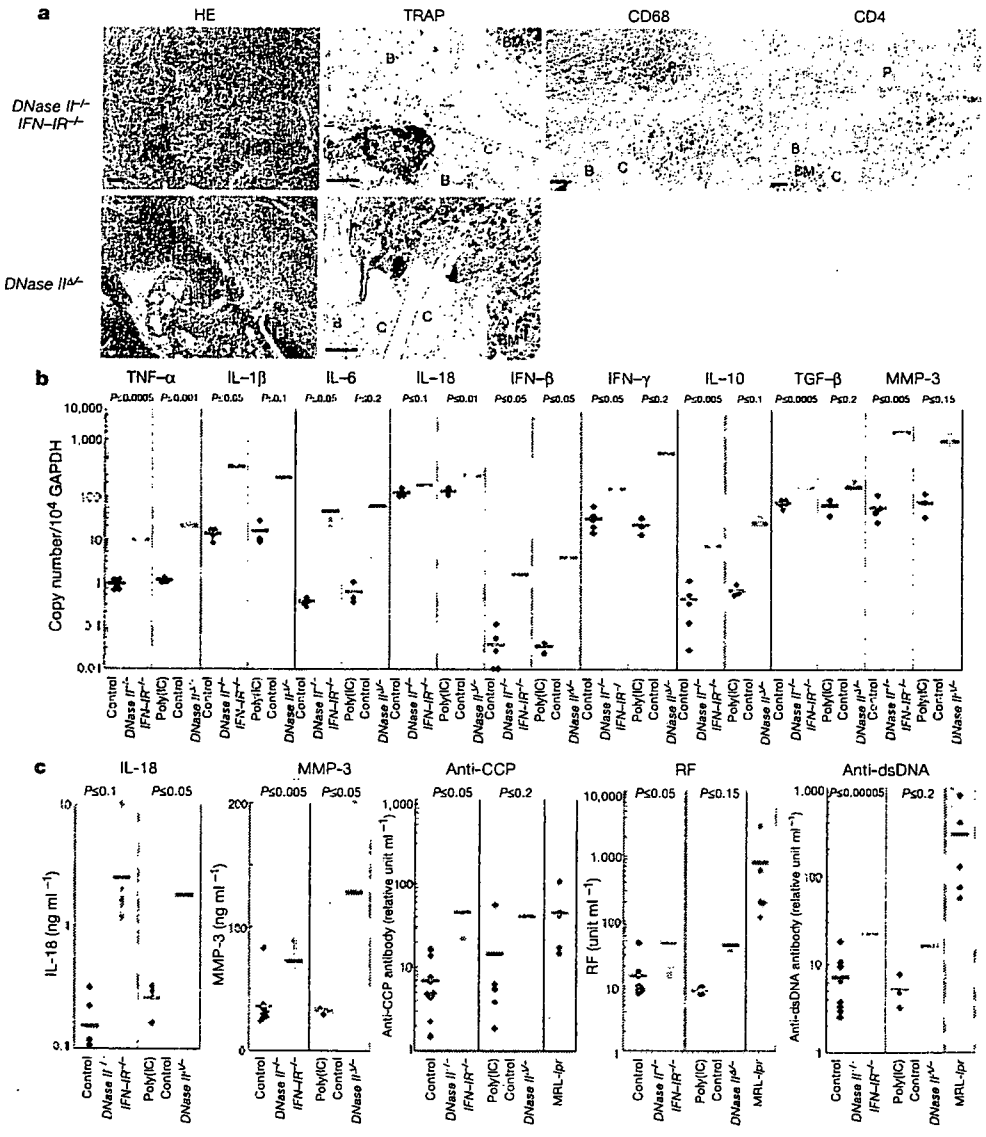


**Figure 2 | Inflammatory arthritis in *DNase II*$^{-/-}$*IFN-IR*$^{-/-}$ mice.** **a**, Joint sections from 8–16.5-month-old *DNase II*$^{-/-}$*IFN-IR*$^{-/-}$ or *DNase II*$^{flox/-}$ mice 10 months after treatment with poly(I)•poly(C) were stained with haematoxylin/eosin (HE), TRAP, anti-CD68 and anti-CD4. P, pannus; B, bone; C, cartilage; BM, bone marrow. Scale bar, 50 μm. **b**, RNAs were prepared from the joints of 7.5–13.5-month-old control or *DNase II*$^{-/-}$*IFN-IR*$^{-/-}$, and those of poly(I)•poly(C)-treated *DNase II*$^{flox/+}$ (poly(IC) control) or *DNase II*$^{\Delta/-}$ mice. The mRNA levels for the indicated cytokines quantified by real-time PCR are expressed relative to mRNA for glyceraldehyde-3-phosphate dehydrogenase (GAPDH). **c**, The concentrations of IL-18, MMP-3, anti-CCP, rheumatoid factor (RF) and anti-dsDNA in the sera from 7.5–16.5-month-old control or *DNase II*$^{-/-}$*IFN-IR*$^{-/-}$, and from poly(I)•poly(C)-treated *DNase II*$^{flox/+}$ or *DNase II*$^{\Delta/-}$ mice are shown. Some parameters were determined for 3–7.5 month-old MRL-*lpr* mice. In **b** and **c**, horizontal red lines indicate the average values. Welch's *t*-test was used to test for difference, and *P* values are shown.

which is specifically observed in human patients with rheumatoid arthritis[11], and rheumatoid factor were also detected at high levels in the serum of *DNase II*$^{-/-}$*IFN-IR*$^{-/-}$ and *DNase II*$^{\Delta/-}$ mice (Fig. 2c). The level of anti-double-stranded DNA (dsDNA) antibody in *DNase II*$^{-/-}$*IFN-IR*$^{-/-}$ mice was about threefold that in wild-type mice, but this value was less than one-tenth of that observed in *lpr* mice, which develop an autoimmune disease similar to systemic lupus erythematosus[12].

*DNase II*$^{-/-}$*IFN-IR*$^{-/-}$ and *DNase II*$^{\Delta/-}$ mice were slightly anaemic (hematocrit 40–45) and had clear growth retardation (data not shown). They developed splenomegaly from the age of 1 month, which became prominent as the mice aged; the weight of the spleen of 7.5–16.5-month-old *DNase II*$^{-/-}$*IFN-IR*$^{-/-}$ mice was about fivefold that of control mice (Fig. 3a). Splenomegaly was due to enlargement of the red pulp. We and others have reported previously that fetal liver and thymus of *DNase II*$^{-/-}$ mice contain many abnormal macrophages carrying undigested DNA from erythroid precursor cells or apoptotic cells[3,4,13]. Similarly, numerous abnormal macrophages carrying DNA in lysosomes were found in bone marrow, spleen and other tissues of the adult *DNase II*$^{-/-}$*IFN-IR*$^{-/-}$ and *DNase II*$^{\Delta/-}$ mice (Fig. 3b). In addition, the serum of 4–6-week-old *DNase II*$^{-/-}$*IFN-IR*$^{-/-}$ mice contained about 10 μg ml$^{-1}$ DNA, and this level decreased as the mice aged (Fig. 3c). *DNase II*$^{\Delta/-}$ mice also carried a low but significant level of DNA in their serum. It is likely that the undigested DNA leaked from the macrophages into the bloodstream.

Cytokines can affect the pathogenesis of human rheumatoid arthritis[7]; we therefore examined the involvement of cytokines in our model. In comparison with that of control mice (less than 20 pg ml$^{-1}$), the serum concentration of TNF-α in *DNase II*$^{-/-}$*IFN-IR*$^{-/-}$ mice was higher (about 100 pg ml$^{-1}$) at 4–6 weeks of age (Fig. 3d), before the joints showed any apparent abnormality. A similar high concentration of TNF-α was observed in *DNase II*$^{\Delta/-}$ mice. In contrast, other cytokines, such as IL-6, IL-1β, IFN-γ, granulocyte/macrophage colony-stimulating factor and IL-4 were undetectable in the serum of *DNase II* mutant mice. We previously reported that the fetal liver of *DNase II*$^{-/-}$ embryos constitutively expresses various cytokines[14]. Real-time PCR indicated that the level of mRNA for TNF-α in the bone marrow of 1-month-old *DNase II*$^{-/-}$*IFN-IR*$^{-/-}$ mice was twice that the level in age-matched control mice (Fig. 3e).

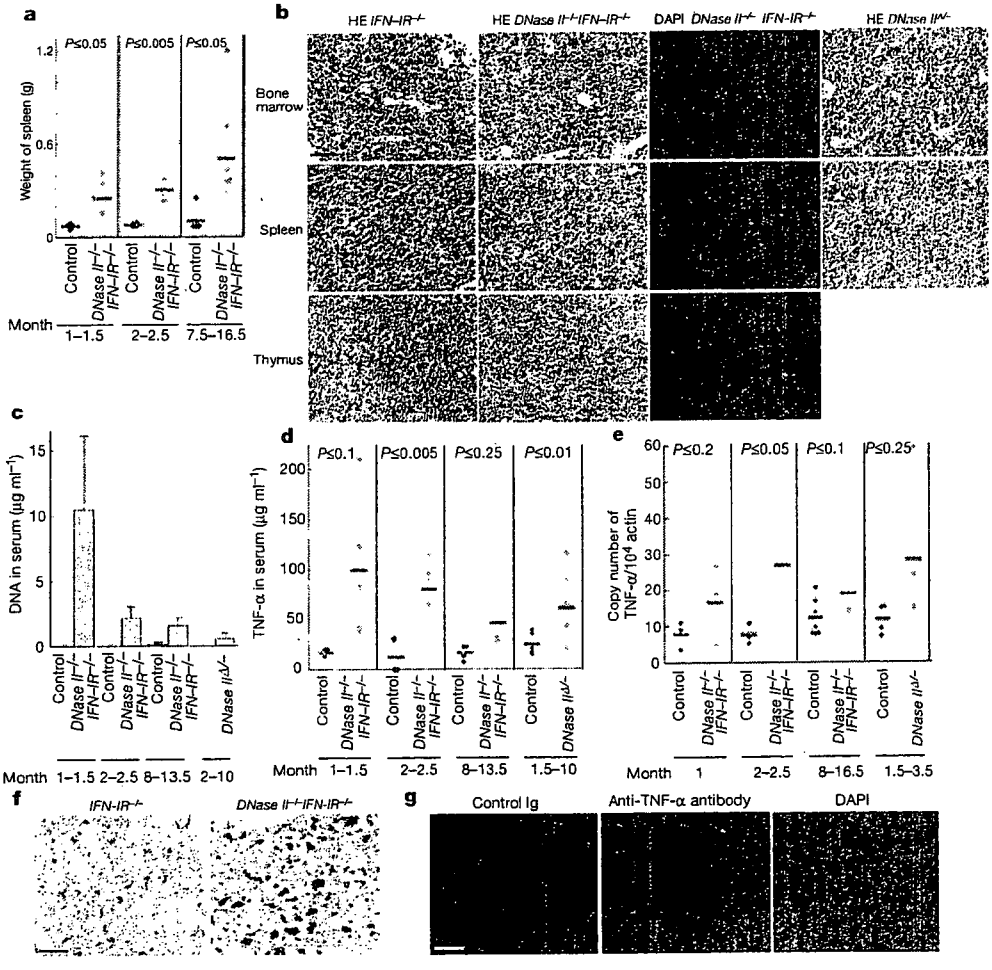


**Figure 3 | Abnormal macrophages.** **a**, The weight of spleens from control and *DNase II*$^{-/-}$*IFN-IR*$^{-/-}$ (four to seven mice) at the indicated ages. **b**, Bone marrow, spleen and thymus of 4–8-week-old *IFN-IR*$^{-/-}$ and *DNase II*$^{-/-}$*IFN-IR*$^{-/-}$ and *DNase II*$^{\Delta/-}$ mice 10 months after treatment with poly(I)•poly(C) were stained with haematoxylin/eosin stain (HE) or 4′,6-diamidino-2-phenylindole (DAPI). Scale bar, 50 μm. **c**, DNA concentration in the serum of control, *DNase II*$^{-/-}$*IFN-IR*$^{-/-}$ and *DNase II*$^{\Delta/-}$ mice (two to six animals for each) at the indicated ages. Results are plotted as means and s.d. **d**, Serum TNF-α concentration of control and *DNase II*$^{-/-}$*IFN-IR*$^{-/-}$, and *DNase II*$^{\Delta/-}$ and *DNase II*$^{flox/+}$ littermates after treatment with poly(I)•poly(C) (three to six mice for each). **e**, mRNA for TNF-α in the bone marrow of control and *DNase II*$^{-/-}$*IFN-IR*$^{-/-}$, and that of poly(I)•poly(C)-treated *DNase II*$^{\Delta/-}$ and *DNase II*$^{flox/+}$ littermates, quantified by real-time PCR, expressed relative to mRNA for β-actin. **f**, Bone marrow from 2-month-old *IFN-IR*$^{-/-}$ and *DNase II*$^{-/-}$*IFN-IR*$^{-/-}$ mice were stained with anti-CD68. Scale bar, 50 μm. **g**, Bone marrow from 1.5-month-old *DNase II*$^{-/-}$*IFN-IR*$^{-/-}$ mice were stained with goat normal IgG or anti-mouse TNF-α. The DAPI staining profile is also shown. Scale bar, 50 μm. In **a**, **d** and **e**, horizontal red lines indicate the average values. Welch's *t*-test was used to test for difference, and *P* values are shown.

The level of mRNA for TNF-α had increased further in these mutant mice by the age of 2–2.5 months, when definitive erythropoiesis is still active. A similar high level of mRNA for TNF-α was found in the bone marrow of *DNase II*$^{\Delta/-}$ mice. Immunohistochemical analyses of the bone marrow (Fig. 3f) showed that the number of macrophages carrying the CD68 antigen in *DNase II*$^{-/-}$*IFN-IR*$^{-/-}$ mice did not differ significantly from that in control mice. However, CD68 was more intensely labelled in *DNase II*$^{-/-}$*IFN-IR*$^{-/-}$ mice, indicating that the macrophages carrying undigested DNA might have been activated[15]. Accordingly, TNF-α was detected in the cells carrying DNA (Fig. 3g).

To determine the effect of blocking TNF-α during the induction of arthritis, 4-week-old *DNase II*$^{-/-}$*IFN-IR*$^{-/-}$ or *DNase II*$^{+/-}$*IFN-IR*$^{-/-}$ littermates were given the neutralizing anti-TNF-α twice a week. *DNase II*$^{-/-}$*IFN-IR*$^{-/-}$ mice that received phosphate-buffered saline (PBS) started to develop arthritis when they were 8–14 weeks old (Fig. 4a). Accordingly, the serum MMP-3 level increased significantly (Fig. 4b). In contrast, mice treated with anti-TNF-α did not develop arthritis at this age, and their serum MMP-3 level was comparable to or slightly higher than that of *DNase II*$^{+/-}$*IFN-IR*$^{-/-}$ control mice. The expression of mRNA for TNF-α, IL-1β, IL-6 and MMP-3 at the joints was also blocked by the anti-TNF-α (Fig. 4c).

We then examined the therapeutic effect of anti-TNF-α after *DNase II*$^{-/-}$*IFN-IR*$^{-/-}$ mice had developed arthritis. Four *DNase II*$^{-/-}$*IFN-IR*$^{-/-}$ mice that showed an arthritis clinical score of 2.5–6 were treated twice a week with anti-TNF-α, and the serum MMP-3 level, which decreases with anti-TNF-α therapy in humans[16], was monitored. As shown in Fig. 4d, after 3 weeks of treatment the serum MMP-3 level had decreased to about one-third of its level before treatment. A decrease in the clinical score of the joints was apparent in two mice. The foot joints were then removed from all the mice, and the cytokine mRNA levels were determined. The joints of *DNase II*$^{-/-}$*IFN-IR*$^{-/-}$ mice receiving PBS carried 5–30-fold the levels of mRNA for TNF-α, IL-6, IL-1β and MMP-3 than those of *DNase II*$^{+/-}$*IFN-IR*$^{-/-}$ control mice, but the mRNA levels in the joints of *DNase II*$^{-/-}$*IFN-IR*$^{-/-}$ mice treated with anti-TNF-α were significantly decreased (Fig. 4e).

Systemic expression of TNF-α in a transgenic mouse model causes the development of chronic polyarthritis, indicating that TNF-α can trigger the disease[17]. Moreover, human patients with rheumatoid arthritis respond well to anti-TNF-α therapy[18,19]. However, the cause of the *TNF-α* gene expression in patients has not been established. We showed that macrophages carrying undigested DNA produce TNF-α, and that anti-TNF-α efficiently blocked the development of polyarthritis in *DNase II*-null mice. It is likely that TNF-α produced by *DNase II*$^{-/-}$ macrophages triggered the pathogenesis by stimulating the growth of synovial cells and by activating cytokine genes in synovial tissues. More than $10^{10}$ red blood cells are generated in the human body every day, and the same number of nuclei are expelled from erythroid precursor cells and degraded by DNase II in bone marrow macrophages. The DNA of apoptotic cells, of which $10^8$–$10^9$ are generated every day, is degraded by DNase II in macrophages. Our results indicate that a failure in this process can lead to the development of polyarthritis. Monocyte activation early in the onset of human rheumatoid arthritis has been noticed in some patients[20]; this is consistent with our results and indicates that the activation of macrophages could be an initiator of the pathogenic cascade in human arthritis. In addition to anti-TNF-α therapy, human patients with rheumatoid arthritis respond to treatment

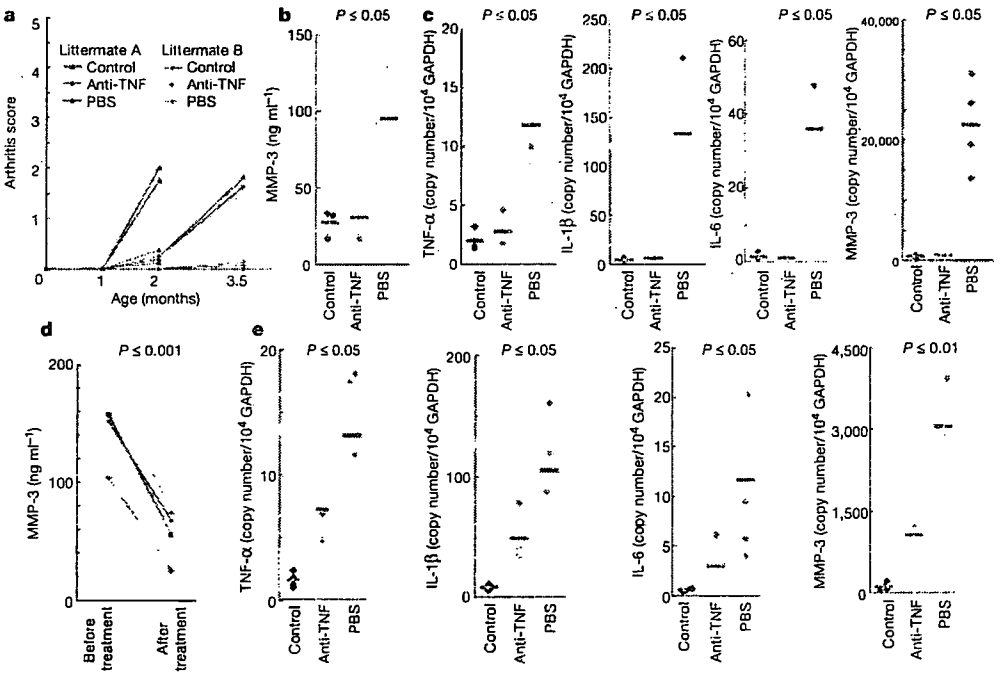


**Figure 4 | Protective and therapeutic effect of anti-TNF-α.**
**a**, *DNase II*$^{-/-}$*IFN-IR*$^{-/-}$ (red and blue results) and *DNase II*$^{+/-}$*IFN-IR*$^{-/-}$ (green results) mice were generated from two litters (shown as triangles and circles). At the age of 1 month, *DNase II*$^{-/-}$*IFN-IR*$^{-/-}$ mice received anti-TNF-α (blue) or PBS (red) twice a week. The clinical score of polyarthritis was determined at the indicated ages. **b**, Serum MMP level in 2-month-old *DNase II*$^{+/-}$*IFN-IR*$^{-/-}$ (control), anti-TNF-α-treated or PBS-treated *DNase II*$^{-/-}$*IFN-IR*$^{-/-}$ (four mice each). **c**, Levels of mRNA for TNF-α, IL-1β, IL-6 and MMP-3 in the joints of the forefoot from 2–4-month-old *DNase II*$^{+/-}$*IFN-IR*$^{-/-}$, anti-TNF-α-treated or PBS-treated *DNase II*$^{-/-}$*IFN-IR*$^{-/-}$ mice expressed relative to mRNA for glyceraldehyde-3-phosphate dehydrogenase (GAPDH).
**d**, **e**, *DNase II*$^{-/-}$*IFN-IR*$^{-/-}$ mice 5–13 months old showing a clinical score of 2.5–6.0 were treated twice a week with anti-TNF-α. **d**, The serum MMP-3 level was determined before and after the 3-week treatment. **e**, Levels of mRNA for TNF-α, IL-1β, IL-6 and MMP-3 in the joints of *DNase II*$^{+/-}$*IFN-IR*$^{-/-}$ (control) and anti-TNF-α-treated or untreated mice were determined after 6 weeks. In **b**, **c** and **e**, horizontal red lines indicate the average values. Welch's *t*-test was used to test for difference, and *P* values are shown.

targeting other pro-inflammatory cytokines, or lymphocytes[21–23]. Whether these treatments are also effective for the polyarthritis in *DNase II*-null mice remains to be studied.

We found DNA in the serum of *DNase II*-deficient mice. Injection of bacterial or mitochondrial DNA into joints induces arthritis, which is mediated by TNF-α produced by macrophages in the joints[24,25]. Immune complexes containing self-DNA activate rheumatoid-arthritis-specific B cells[26]. In these cases, Toll-like receptor 9 (TLR9) is necessary for activating the *TNF-α* gene in macrophages and for producing rheumatoid factor in B cells. In contrast, deletion of the *TLR9* gene had no apparent effect on the development of arthritis in *DNase II*$^{-/-}$ *IRF-IR*$^{-/-}$ mice (K.K. and S.N., unpublished observations), indicating that DNA in the serum might not contribute to the pathogenesis directly. In contrast, we found that macrophages carrying undigested DNA were activated and produced TNF-α. Our results are consistent with the findings that the fetal liver macrophages in *DNase II*$^{-/-}$ mice express IFN-β and TNF-α by a TLR-independent mechanism[14] and that cytosolic DNA activates the innate immunity through a TLR-independent system[27,28]. Further characterization of this TLR-independent pathway is needed to explain the molecular mechanism by which cells sense the DNA that has escaped from degradation and cause autoimmunity.

## METHODS

**Mice.** Mice deficient in the *DNase II* and *IFN-IR* genes were described previously[5]. *E2a-Cre* (ref. 29) and *Mx1-Cre* transgenic mice[6] were from the Jackson Laboratory. MRL-*lpr* mice were purchased from Japan SLC. The conditional DNase II targeting mice are described in Supplementary Methods. The anti-TNF-α monoclonal antibody (20 μg per g body weight) was administered twice a week by intraperitoneal injection, and clinical parameters were assessed 3 days after the last injection.

**Clinical assessment, and histology.** Swelling of the forelimb and hindlimb joints was inspected manually and scored as follows: 0, no swelling; 1, mild swelling; 2, severe swelling or deformation of the limb or finger. The scores were summed, and a total score (maximum 8) was given to each mouse. The detailed procedures of MRI, radiography and histological analysis are described in Supplementary Methods.

**Enzyme-linked immunosorbent assay (ELISA), real-time PCR and serum DNA.** The serum levels of TNF-α, IL-18, rheumatoid factor and MMP-3 were determined with ELISA kits from Beckton Dickinson, MBL, Shibayagi and R&D Systems, respectively. Anti-dsDNA and anti-CCP were measured with a MESACUP DNA-II test kit (MBL) and a DIASTAT anti-CCP ELISA kit (Axis-Shield), except that peroxidase-conjugated goat antibody against mouse immunoglobulin (Cappel) was used as the detection antibody. The procedure for real-time PCR, the primers and the assay method for serum DNA are described in Supplementary Methods.

**Received 27 July; accepted 14 September 2006.**


1. Nagata, S. DNA degradation in development and programmed cell death. *Annu. Rev. Immunol.* 23, 853–875 (2005).
2. Evans, C. J. & Aguilera, R. J. DNase II: genes, enzymes and function. *Gene* 322, 1–15 (2003).
3. Kawane, K. *et al.* Requirement of DNase II for definitive erythropoiesis in the mouse fetal liver. *Science* 292, 1546–1549 (2001).
4. Kawane, K. *et al.* Impaired thymic development in mouse embryos deficient in apoptotic DNA degradation. *Nature Immunol.* 4, 138–144 (2003).
5. Yoshida, H., Okabe, Y., Kawane, K., Fukuyama, H. & Nagata, S. Lethal anemia caused by interferon-β produced in mouse embryos carrying undigested DNA. *Nature Immunol.* 6, 49–56 (2005).
6. Kuhn, R., Schwenk, F., Aguet, M. & Rajewsky, K. Inducible gene targeting in mice. *Science* 269, 1427–1429 (1995).
7. Feldmann, M., Brennan, F. M. & Maini, R. N. Role of cytokines in rheumatoid arthritis. *Annu. Rev. Immunol.* 14, 397–440 (1996).
8. Firestein, G. S., Alvaro-Gracia, J. M. & Maki, R. Quantitative analysis of cytokine gene expression in rheumatoid arthritis. *J. Immunol.* 144, 3347–3353 (1990).
9. Saxne, T., Palladino, M. A. Jr, Heinegard, D., Talal, N. & Wollheim, F. A. Detection of tumor necrosis factor alpha but not tumor necrosis factor beta in rheumatoid arthritis synovial fluid and serum. *Arthritis Rheum.* 31, 1041–1045 (1988).
10. Manicourt, D. H., Fujimoto, N., Obata, K. & Thonar, E. J. Levels of circulating collagenase, stromelysin-1, and tissue inhibitor of matrix metalloproteinases 1 in patients with rheumatoid arthritis. Relationship to serum levels of antigenic keratan sulfate and systemic parameters of inflammation. *Arthritis Rheum.* 38, 1031–1039 (1995).
11. Schellekens, G. A., de Jong, B. A., van den Hoogen, F. H., van de Putte, L. B. & van Venrooij, W. J. Citrulline is an essential constituent of antigenic determinants recognized by rheumatoid arthritis-specific autoantibodies. *J. Clin. Invest.* 101, 273–281 (1998).
12. Cohen, P. L. & Eisenberg, R. A. *Lpr* and *gld*: single gene models of systemic autoimmunity and lymphoproliferative disease. *Annu. Rev. Immunol.* 9, 243–269 (1991).
13. Krieser, R. J. *et al.* Deoxyribonuclease IIa is required during the phagocytic phase of apoptosis and its loss causes lethality. *Cell Death Differ.* 9, 956–962 (2002).
14. Okabe, Y., Kawane, K., Akira, S., Taniguchi, T. & Nagata, S. Toll-like receptor-independent gene induction program activated by mammalian DNA escaped from apoptotic DNA degradation. *J. Exp. Med.* 202, 1333–1339 (2005).
15. Ramprasad, M. P., Terpstra, V., Kondratenko, N., Quehenberger, O. & Steinberg, D. Cell surface expression of mouse macrosialin and human CD68 and their role as macrophage receptors for oxidized low density lipoprotein. *Proc. Natl Acad. Sci. USA* 93, 14833–14838 (1996).
16. Brennan, F. M. *et al.* Reduction of serum matrix metalloproteinase 1 and matrix metalloproteinase 3 in rheumatoid arthritis patients following anti-tumour necrosis factor-alpha (cA2) therapy. *Br. J. Rheumatol.* 36, 643–650 (1997).
17. Keffer, J. *et al.* Transgenic mice expressing human tumour necrosis factor: a predictive genetic model of arthritis. *EMBO J.* 10, 4025–4031 (1991).
18. Feldmann, M. & Maini, R. N. Anti-TNF alpha therapy of rheumatoid arthritis: what have we learned? *Annu. Rev. Immunol.* 19, 163–196 (2001).
19. Feldmann, M. Development of anti-TNF therapy for rheumatoid arthritis. *Nature Rev. Immunol.* 2, 364–371 (2002).
20. Fujii, I., Shingu, M. & Nobunaga, M. Monocyte activation in early onset rheumatoid arthritis. *Ann. Rheum. Dis.* 49, 497–503 (1990).
21. Edwards, J. C. & Cambridge, G. B-cell targeting in rheumatoid arthritis and other autoimmune diseases. *Nature Rev. Immunol.* 6, 394–403 (2006).
22. Bluestone, J. A., St Clair, E. W. & Turka, L. A. CTLA4Ig: bridging the basic immunology with clinical application. *Immunity* 24, 233–238 (2006).
23. Yokota, S. *et al.* Therapeutic efficacy of humanized recombinant anti-interleukin-6 receptor antibody in children with systemic-onset juvenile idiopathic arthritis. *Arthritis Rheum.* 52, 818–825 (2005).
24. Deng, G. M., Nilsson, I. M., Verdrengh, M., Collins, L. V. & Tarkowski, A. Intra-articularly localized bacterial DNA containing CpG motifs induces arthritis. *Nature Med.* 5, 702–705 (1999).
25. Collins, L. V., Hajizadeh, S., Holme, E., Jonsson, I. M. & Tarkowski, A. Endogenously oxidized mitochondrial DNA induces *in vivo* and *in vitro* inflammatory responses. *J. Leukoc. Biol.* 75, 995–1000 (2004).
26. Leadbetter, E. A. *et al.* Chromatin-IgG complexes activate B cells by dual engagement of IgM and Toll-like receptors. *Nature* 416, 603–607 (2002).
27. Stetson, D. B. & Medzhitov, R. Recognition of cytosolic DNA activates an IRF3-dependent innate immune response. *Immunity* 24, 93–103 (2006).
28. Ishii, K. J. *et al.* A Toll-like receptor-independent antiviral response induced by double-stranded B-form DNA. *Nature Immunol.* 7, 40–48 (2006).
29. Williams-Simons, L. & Westphal, H. EIIaCre—utility of a general deleter strain. *Transgenic Res.* 8, 53–54 (1999).


**Supplementary Information** is linked to the online version of the paper at www.nature.com/nature.

**Acknowledgements** We thank K. Aozasa for pathological analysis of the mice, P. Quartier for critical reading of our manuscript, M. Nishikawa, H. Matsuda, T. Matsuki, A. Seiyama and T. Yanagida for advice and discussion, H. Fukuyama for help at the initial stage of this work, and M. Fujii and M. Harayama for secretarial assistance. This work was supported in part by Grants-in-Aid from the Ministry of Education, Science, Sports, and Culture in Japan.

**Author Information** Reprints and permissions information is available at www.nature.com/reprints. The authors declare no competing financial interests. Correspondence and requests for materials should be addressed to S.N. (nagata@genetic.med.osaka-u.ac.jp).

Research article

Open Access

# Inhibitory effect of ribbon-type NF-κB decoy oligodeoxynucleotides on osteoclast induction and activity *in vitro* and *in vivo*

Yasuo Kunugiza[1,2], Tetsuya Tomita[2], Naruya Tomita[3], Ryuichi Morishita[1] and Hideki Yoshikawa[2]

[1]Division of Clinical Gene Therapy, Osaka University Graduate School of Medicine, 2-2 Yamada-oka, Suita, Osaka 565-0871, Japan
[2]Department of Orthopaedics, Osaka University Graduate School of Medicine, 2-2 Yamada-oka, Suita, Osaka 565-0871, Japan
[3]Division of Nephrology, Department of Internal Medicine, Kawasaki Medical School, 577 Matsushima, Kurashiki, Okayama 701-0192, Japan

Corresponding author: Tetsuya Tomita, tomita@ort.med.osaka-u.ac.jp

Received: 11 Oct 2005 Revisions requested: 1 Dec 2005 Revisions received: 27 Feb 2006 Accepted: 29 May 2006 Published: 3 Jul 2006

*Arthritis Research & Therapy* 2006, 8:R103 (doi:10.1186/ar1980)
This article is online at: http://arthritis-research.com/content/8/4/R103


## Abstract

In this study we examined the effect of ribbon-type (circular-type) NF-κB decoy oligodeoxynucleotides (RNODN) on osteoclast induction and activity. We extracted bone marrow cells from the femurs of rats and incubated non-adherent cells with receptor activator of nuclear factor κB ligand (RANKL) and macrophage colony-stimulating factor (M-CSF). First, transfer efficiency into osteoclasts and their precursors, resistance to exonuclease, and binding activity of decoy to NF-κB were examined. Next, to examine the effect of RNODN on osteoclast induction and activity, osteoclast differentiation and pit formation assays were performed. RNODN were injected into the ankle joints of rats with collagen-induced arthritis. Joint destruction and osteoclast activity were examined by histological study. The resistance of RNODN to exonuclease and their binding activity on NF-κB were both greater than those of phosphorothionated NF-κB decoy oligodeoxynucleotides. The absolute number of multinucleate cells scoring positive for tartrate-resistant acid phosphatase was significantly decreased in the RNODN-treated group. The average calcified matrix resorbed area was significantly decreased in the RNODN-treated group. Histological study showed marked suppression of joint destruction and osteoclast activity by intra-articular injection of RNODN. These results suggest the inhibitory effect of RNODN on the induction and activity of osteoclasts. Direct intra-articular injection of RNODN into the joints may be an effective strategy for the treatment of arthritis.

## Introduction

Osteoclasts are multinucleate giant cells formed by the fusion of hematopoietic cells of the monocyte/macrophage lineage. They are the major resorptive cells of bone [1,2]. In the differentiation pathway of osteoclast progenitors into functionally active osteoclasts, macrophage colony-stimulating factor (M-CSF) is important in proliferation; both M-CSF and receptor activator of NF-κB ligand (RANKL) are essentially involved in differentiation, survival, and fusion; and RANKL enhances osteoclast function [3,4]. The expression of RANKL can be observed in synovial fibroblasts from patients with rheumatoid arthritis (RA) [5]. A crucial target of signaling by RANKL is the activation of NF-κB [6-9]. NF-κB is associated with the activation of osteoclasts and is important in the differentiation of osteoclast precursors [10]. Several studies indicate that selective inhibition of NF-κB in osteoclast precursors prevents osteoclast differentiation and function *in vitro* and *in vivo* [11,12]. Mice deficient in both the p50 and p65 subunits of NF-κB develop osteopetrosis because of a defect in osteoclast differentiation [13,14]. Recently the importance of the IκB kinase (IKK) β subunit as a transducer of signals from RANK to NF-κB for inflammation-induced bone loss and osteoclastogenesis *in vivo* was reported [15].

RA is a chronic inflammatory disease of unknown etiology, characterized by articular inflammation associated with

FCS = fetal calf serum; FITC = fluorescein isothiocyanate; IL = interleukin; M-CSF = macrophage colony-stimulating factor; NF-κB = nuclear factor-κB; ODN = oligodeoxynucleotide; PBS = phosphate-buffered saline; PNODN = phosphorothionate double-stranded NF-κB decoy ODN; PSODN = phosphorothionate double-stranded scrambled decoy ODN; RA = rheumatoid arthritis; RANKL = receptor activator of NF-κB ligand; RNODN = ribbon-type NF-κB decoy ODN; RSODN = ribbon-type scrambled decoy ODN; TNF = tumor necrosis factor; TRAP = tartrate-resistant acid phosphatase.